Master's thesis

NTNU
Norwegian University of Science and Technology
Faculty of Information Technology and Electrical Engineering
Department of Mathematical Sciences

Jens Georg Berg-Jensen

Adaptive Monitoring of Snowpack Development using a Dynamic Linear Model.

A data-driven approach to monitor snowpack stability over time.

Master's thesis in Natural Science with Teacher Education
Supervisor: Jo Eidsvik
June 2021

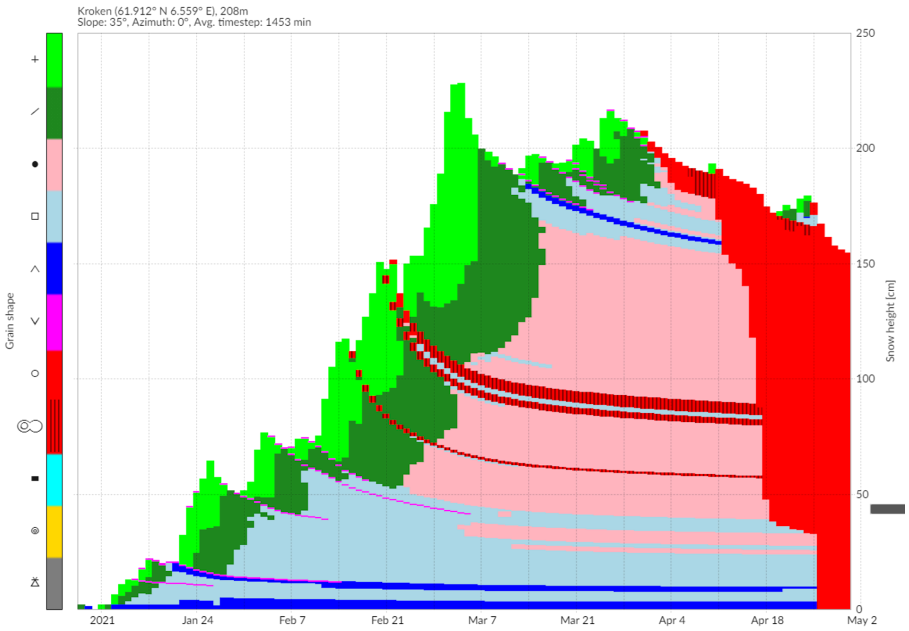

NTNU
Norwegian University of Science and Technology

Jens Georg Berg-Jensen

Adaptive Monitoring of Snowpack Development using a Dynamic Linear Model.

A data-driven approach to monitor snowpack stability over time.

Master's thesis in Natural Science with Teacher Education
Supervisor: Jo Eidsvik
June 2021

Norwegian University of Science and Technology
Faculty of Information Technology and Electrical Engineering
Department of Mathematical Sciences

Abstract

Snow avalanches are among the most frequent natural hazard events in Norway, posing a significant threat to human life and a major problem for infrastructure, as avalanches are among the most common causes of roadblocks. Varsom[1] is a monitoring/warning system developed to predict avalanche danger, relying on weather data, manual stability tests, and earlier avalanche activity in an area. This thesis develops a statistical model that predicts the stability of the weakest layer in a snowpack based on numerical snow cover simulations, weather data, and drone measurements. The numerical data are calculated with the program SNOWPACK and includes two stability measures of each layer in a simulated snowpack, SK_{38} and SSI. SSI is used to locate weak layers in a snowpack, while SK_{38} indicates the stability of a weak layer.

An adaptive dynamic linear model is developed to model snow properties over time sequentially and predict the stability measure SK_{38} of the weak layer, with its uncertainty. The snow properties modeled are the weak layer thickness, density, grain size, and bond size, and new snow thickness and density. The weather input data are temperature, precipitation, and wind speed. The model parameters are dynamic, depending on the weather regime on a particular day. The formulation of the model facilitates experimental design and planning. In particular, the model initiates drone measurements when necessary and updates the model distribution with the new measurements. Two strategies for drone data gathering are developed and compared with a model that does not rely on new drone measurements. The first is an Adaptive Monitoring strategy, which initiates drones when there is less than 90 % probability that the predicted stability of a weak layer is above a threshold. The second strategy is a Value of Information strategy, which initiates drones when the expected value of a drone measurement is higher than a threshold.

The stability predictions of the adaptive models had less uncertainty than for the non-adaptive model, especially directly after a drone measurement. The non-adaptive model was generally pessimistic with its predictions. The two adaptive strategies resulted in a similar number of drone events, with a fixed stability threshold. An increase in the stability threshold leads to an increase in drone events for the Adaptive Monitoring strategy. An increase in the cost associated with keeping a road open when the predicted stability was lower than a threshold leads to more drone events for the Value of Information strategy.

[1] https://www.varsom.no/snoskredvarsling/?ref=mainmenu

Sammendrag

Snøskred er en av de mest vanlige naturfarene i Norge, med stor trussel mot menneskeliv og infrastruktur, siden snøskred er en av de vanligste årsakene for blokkering av veier. Varsom er et overvåkings og varslingssystem utviklet for å forutsi snørasfare, basert på værdata, manuelle stabilitetstester og tidligere skredaktivitet i et område. Denne avhandlingen utvikler en statistisk modell som forutsier stabiliteten til det svakeste laget i snødekke, basert på numeriske snødekkesimuleringer, værdata og dronemålinger. De numeriske dataene er kalkulert med programmet SNOWPACK, og inkluderer to mål på stabilitet av hvert lag i et simulert snødekke, SK_{38} og SSI. SSI blir brukt til å lokalisere svake lag i snødekke, mens SK_{38} indikerer stabiliteten til et svakt lag.

En adaptiv dynamisk lineær modell er utviklet til å sekvensielt modellere snø-egenskaper over tid og forutsi stabiliteten SK_{38} av det svake laget, med dets usikkerhet. Snø-egenskapene som modelleres er det svake lagets tykkelse, tetthet, kornstørrelse og bindingsstørrelse, og nysnøens tykkelse og tetthet. Værdataen som blir brukt som input er temperatur, nedbør og vindhastighet. Modellparameterne er dynamiske, og avhenger av værregimet på en bestemt dag. Modellens formulering tilrettelegger for eksperimentell design og planlegging. Spesielt setter modellen i gang dronemålinger når det er nødvendig, og oppdaterer fordelingsfunksjonen til modellen basert på de nye målingene. To strategier for dronedata-innsamling er utviklet og sammenlignet med en modell som ikke er avhengig av nye drone-målinger. Den første er en adaptiv overvåkingsstrategi, som starter dronemålinger når det er mindre enn 90 % sannsynlighet for at den forventede stabiliteten til det svake laget er over en terskel. Den andre strategien er en Informasjonsverdi-strategi, som setter i gang dronemålinger når den forventede verdien av å samle inn en dronemåling er høyere enn en terskel.

Stabilitetsforutsigelsene til de to adaptive modellene hadde mindre usikkerhet enn den adaptive modellen, spesielt direkte etter en dronemåling. Den ikke-adaptive modellen var generelt pessimistisk med sine forutsigelser. De to adaptive strategiene resulterte i et tilsvarende antall dronehendelser, når stabilitetsterskelen var konstant. En økning i stabilitetsterskelen førte til en økning i antall dronehendelser for den adaptive overvåkingsstrategien. En økning i kostnadene knyttet til å holde en vei åpen når den forventede stabiliteten var lavere enn en terskel, førte til et større antall dronehendelser med Informasjonsverdi-strategien.

Preface

This thesis concludes the Master of Science degree in Statistics. It is written for the Department of Mathematical Sciences at the Norwegian University of Science and Technology (NTNU). The project constitutes 30 credits in the tenth semester of the Natural Science with Teacher Education study program, written in the spring of 2021. The thesis has increased my understanding of applying mathematics to solve real-life problems, which will help me as a teacher to motivate the students.

First of all, I want to thank my supervisor Jo Eidsvik for his supervision and guidance throughout this semester. The weekly meetings were both motivating and sometimes necessary for the progress of the thesis, especially during the strictest lockdown in Trondheim. I also want to thank the GeoDrone-team at SINTEF-Petroleum, Arnt Grøver, Bastien Dupuy, and Anouar Romdhane, for biweekly meetings and the inputs discussions and guidance during the whole semester. This helped me understand the problem and narrow down the scope of the thesis. Lastly, I would like to thank my closest friends and family for their guidance, support, and motivation.

Jens Georg Berg-Jensen
Trondheim, June 01, 2021

Contents

List of Figures

List of Tables

Chapter 1

Introduction

1.1 Motivation

Snow avalanches occur in areas with terrain suitable for avalanche formation, corresponding to approximately 7 % of Norway. They pose a significant threat to human life and are a major problem for infrastructure, as avalanches are among the most common causes of roadblocks. Every winter, roads, and railways are closed as a consequence of snow avalanches. Suppose a road is a sole connection between towns or regions and has no alternative roads. In that case, a roadblock can have severe economic consequences and also lead to the isolation of small towns (Norges Geotekniske Institutt [NGI], n.d.; Statens Vegvesen, 2014).

A robust warning and monitoring system, called **Varsom**, has been developed to reduce the impact of snow avalanches in Norway. The system is developed by NVE (The Norwegian Water Resources and Energy Directorate), in partnership with The Norwegian Public Roads Administration and the Norwegian Meteorological Institute. Varsom forecasts the avalanche danger at a location for the next two days, based on weather data, manual snow stability observations, and earlier avalanche activity (Norges Vassdrag- og Energidirektorat [NVE], 2021).

The formation and development of a layered snowpack over time is an essential factor in snow avalanche formation. After a snowfall, a new layer adds to the snowpack, with different snow properties than the other layers in the snowpack. The layer properties change over time due to external and internal conditions, increasing the snowpack's complexity. Layers weakly bonded with the overlying and underlying snow are called weak layers. A slab avalanche is an avalanche caused by a weak layer collapsing due to an increased load on top of the layer, resulting in the overlying slab falling down the slope. The additional load could be a human on the snowpack surface or a natural trigger such as a high amount of new snow (Müller, 2019a).

Monitoring the development of a weak layer and its stability over time is vital for

the avalanche warning systems, requiring continuous monitoring and testing (Müller, 2019a). A problem in Norway is the low number of available data stations relative to alpine countries like Switzerland. There are numerous automatic weather stations monitoring weather conditions, but only a few monitor snow data, such as snow temperature and depth. Manual observation is the usual way to monitor snowpacks and weak layers in Norway. Stability tests, such as compression tests and hardness tests, are done by several testers in different parts of Norway. Volunteers are also encouraged to send in data (pictures, snow information) at **Regobs**[1], a service provided by Varsom.

Numerical modeling of snowpacks in support of avalanche forecasting is a growing area within Geoscience. A numerical model simulates a developing snowpack over time, based on meteorological data from automatic weather stations, numerical weather prediction, or climate models. This provides information otherwise unavailable to a forecaster, including properties and stability measures of each layer in the snowpack (Mayer et al., 2021; Viallon-Galinier et al., 2021). One of the most widely used numerical models is the detailed snowpack model SNOWPACK[2], developed by WSL Institute for Snow and Avalanche Research SLF (SLF, n.d.-c). This model makes it possible to simulate the full development of a snowpack over a winter period. A challenge with SNOWPACK is its relatively high computation cost. Also, even though its physical representation eases the interpretations of cause and effect, it is difficult to modify the results coherently, say with uncertain snow measurements.

Different approaches have been made to predict weak layer stability based on the stability measure calculated by SNOWPACK. No quantitative stability measures can give an absolute indicator for snowpack stability, given the complex nature within a layered snowpack (Viallon-Galinier et al., 2021). Some results verify stability patterns between numerical predictions and manual observations. Mayer et al. (2021) trained a random forest model on a combination of mechanical stability metrics, weak layer properties, and overlying slab properties to predict the probability of an unstable layer in a snowpack with valid results. An article by Bellaire et al. (2006) demonstrated that the stability metrics SK_{38} and SSI, as calculated by SNOWPACK, added support to stability evaluation and suggested that a combination of SK_{38} and SSI reproduces observed stability patterns.

A way to obtain additional snow data at a location is by drone monitoring. Drones equipped with sensors such as Ground Penetrating Radar (GPR), high-resolution cameras, and Light Detection and Ranging (LIDAR) can retrieve snow depth, layer thickness, snow density, and possibly other properties in a snowpack. Utilizing drones could limit the need for manual observations in avalanche-prone areas, limiting the amount of dangerous manual inspections, potentially saving human life. Drone monitoring also allows to cover wide areas and accounts for spatial variability. An example of practical use of a drone measurement is when a snowpack is deemed potentially

[1] https://regobs.no
[2] https://models.slf.ch/p/snowpack/

unstable. For instance, after an avalanche, a drone could monitor the remaining snowpack for possible sub-avalanches.

Combining the available data from manual observations, numerical models, and drone measurements provide a considerable increase of available data. Such data is essential for the development of data-driven statistical models and their applicability in Norway. Reliable updating would be much easier in a setting with a statistical model, which naturally leads to uncertainty statements. Some data-driven models that can be implemented include time series models that monitor stability over time and machine learning models that estimate a probability of an avalanche occurring at a location. Data-based approaches are getting more popular in the field and are a major focus area for the development of warning systems in Norway (NVE, 2021).

1.2 Goal

The model developed in this thesis is a dynamic time series model that estimates snow properties and uses the properties to predict weak layer stability. It uses adaptive strategies to initiate drones that measure the snow properties and updates the model distribution with new measurements. The model is an adaptive data-driven sequential model called a Dynamic Linear Model (DLM). The DLM models new snow density and thickness and weak layer density, thickness, grain size, and bond size over time. The purpose is to use the snow properties the previous day to one-step forecast the next day's properties. The model parameters change dynamically according to the weather regime on a specific day. The statistical model is trained from SNOWPACK data and weather data and updates with drone data. The primary goal is a model that can predict the weak layer stability based on the available data and initiate drone measurements when a weak layer needs closer monitoring.

Two different adaptive strategies are implemented to initiate drones, obtaining accurate measurements of the snowpack properties. The first strategy is an AMA strategy (Adaptive Monitoring Algorithm), where the model initiates a drone when there is less than 90 % probability that the predicted stability is above a threshold. The second strategy is a VOI strategy (Value of Information), where the model initiates a drone if the value of a drone measurement is higher than a threshold. Both strategies update the model distribution based on the drone measurements, utilizing the Bayesian framework.

The adaptive strategies used to initiate the drone has a practical application in deciding when a drone measurement is necessary. The model also extends the available information to a forecaster by applying additional data sources less common in the Norwegian warning systems, such as numerical models and drone measurements. This contributes to the warning systems in Norway, especially for avalanche events such as slab avalanches that rely on snowpack stability.

The chosen study area is two locations in Stryn, called Kroken and Fjellet, in Vestland Fylke. Kroken is approximately 200 meters over sea level, while Fjellet is approximately 1000 meters over sea level. Both locations are close to national road Rv. 15, an important transport route between Norway's eastern and western parts. The road passes the mountain range Strynefjellet, an avalanche-prone area due to weather and terrain (Statens Vegvesen, 2014). WxGen[3] is used to generate the weather required to simulate the snowpack with SNOWPACK. WxGen is a weather scenario generator developed by the Norwegian Meteorological Institute (Norwegian Meteorological Institute [MI], n.d.). The weather is generated in both locations in the period January 1 to April 30, 2021.

1.3 Structure of thesis

Chapter 2 presents a theoretical overview of snow metamorphism, snowpack stability, and snow avalanche formation. It also introduces the numerical snowpack simulation program SNOWPACK, the weather generator program WxGen, and the project GeoDrone. Chapter 3 is an introduction to DLM and the sequential procedure utilized in the thesis. Chapter 4 introduces the adaptive strategies AMA and VOI used to initiate the drone measurements. Chapter 5 presents the data generation part of the project, which is used in the analysis. In Chapter 6 the adaptive dynamic linear model is applied to the data, and the results are analyzed. The results, limitations, and further works of the model are discussed in Chapter 7.

[3]https://github.com/metno/wxgen

Chapter 2

Snow Stratigraphy

This chapter introduces the main geophysical theory relevant for snowpack development and snow avalanche formation. The focus is *snow stratigraphy*, which concerns the properties and internal processes occurring within a layered structure of snow (Pielmeier & Schneebeli, 2003). In Chapter 2.1 the formation of a layered snowpack and the processes within the snowpack are introduced. Chapter 2.2 introduces some of the most important processes leading to snow avalanche formation, including theory on the stability of the weak layer in the snowpack. The mechanical stability measures SSI and SK_{38} are presented and discussed in Chapter 2.3. Chapter 2.4 introduces the numerical model SNOWPACK and the weather generator WxGen. Chapter 2.5 presents the use of drone measurements.

2.1 Snow formation and metamorphism

Precipitation takes the form of snow when the atmospheric temperature is at or below freezing temperature (National Snow and Ice Data Center [NSICD], n.d.). The water droplets in the clouds are considered supercooled, and the water vapor freezes, forming snow crystals. A snow crystal consists of around 100 trillion water molecules, and the structure and form of a snow crystal are determined by the water molecules' location on the crystal, making every crystal uniquely constructed. While falling towards the ground, external conditions such as temperature, wind, and humidity affect the crystals' structure and properties. Some crystals take the form of a pointed star, while others take the form of sleet. Snow is an accumulation of snow crystals on the ground, and its structure and properties depend accordingly on the crystals' structure and properties (Müller, 2019a; SLF, n.d.-d).

At first glance, snow looks like a monotonous structure, but by digging deeper into the snowpack, a layered structure appears. On the bottom lies the oldest layer, the snowpack's beginning. A new layer appears on top after a snowfall, adding to the snowpack's complexity. Each layer consists of different snow grains, but the primary type of snow grain in a layer gives its categorical name. Table 1 shows the

different kinds of layers in a snowpack. The properties and structure of each layer change continuously due to a process called *snow metamorphism*. Snow metamorphism concerns the transformation in each layer and the overall snowpack evolution. Snow is thermodynamically unstable because it exists close to its triple point where solid, liquid, and vapor exist simultaneously. This leads to constant changes in the structure and properties of snow, either by melting or by freezing processes (American Avalance Center & National Avalanche Center [AAC], n.d.-a; SLF, n.d.-a). The snow temperature at the snowpack surface is quite different from the snow temperature close to the ground, resulting in large vapor pressure differences across the snowpack. Water vapor generally flows from areas with high pressure (warm areas) to areas with low pressure (cold areas) within the snowpack (Müller, 2019a).

The main processes of snow metamorphism are rounding and faceting of snow. Rounding is the decomposition of snow crystals into rounder grains, a process beginning immediately after a snowfall. The pointy, convex areas of a snow crystal are more susceptible to pressure than the concave areas, so the snow grains decompose to rounder forms. Rounded grains are small in volume and have strong bonds. The rounding process occurs when the temperature gradient in the snowpack is low, resulting in slow water vapor flow from the warm areas to the cold areas within the snowpack. Rounding also occurs in windy conditions, as wind-drifted snow crystals get rounded by contact with other snow grains or with the snowpack surface, resulting in rounded and dense grains (Müller, 2019b; Statens Vegvesen, 2014).

Faceting happens in snowpacks with large temperature gradients, as water vapor flows quickly from the warm areas to the cold areas of the snowpack. The water vapor condenses on the crystals in the cold areas resulting in large and angular crystals, called faceted crystals. Snow consisting of faceted crystals has weak bonds and strength and typically low density. Suppose the temperature gradient stays high over a long period. In that case, the crystals develop into hollow, cup-shaped crystals, resulting in a layer called depth hoar (see Table 1) (Mayer et al., 2021; Müller, 2019a).

Melt/freeze cycles are central processes in the evolution of a snowpack. If the snow temperature is close to 0 °C, the snow melts. The evaporated water settles in the spaces between the snow grains, weakening the bonds and creating bigger snow grains. Freezing temperatures lead to snow turning to ice, creating fixed bonds. When this happens on the snowpack surface, it creates a crust. These crusts have a crystal structure with weak bonds to adjacent layers. After a new snowfall buries the crust, the crust develops weak bonds with the new snow. A usual consequence of melt/freeze cycles is a layer consisting of faceted crystals with weak bonds, with an ice crust on the top. The ice crust acts as a vapor barrier and thus supports faceting under the crust. The layer of faceted crystals is then usually denoted as a weak layer (Mayer et al., 2021; Müller, 2019a).

Figure 1 depicts the rounding processes, faceting processes, and melt/freeze pro-

	Grain Type	Description
PP	New Snow Particles	New snow
FC	Faceted Crystals	Large grained, weak bonds
DF	Fragmented New Snow Particles	Rounded New Snow
DH	Depth Hoar	Large grains, weak bonds
RG	Rounded Grains	Small grains, strong bonds
SH	Surface Hoar	Large grains, weak bonds, thin layer
MF	Melt forms	Wet snow

Table 1: The different snow grain types found in a snowpack, with a description of the most relevant properties.

cesses in a snowpack.

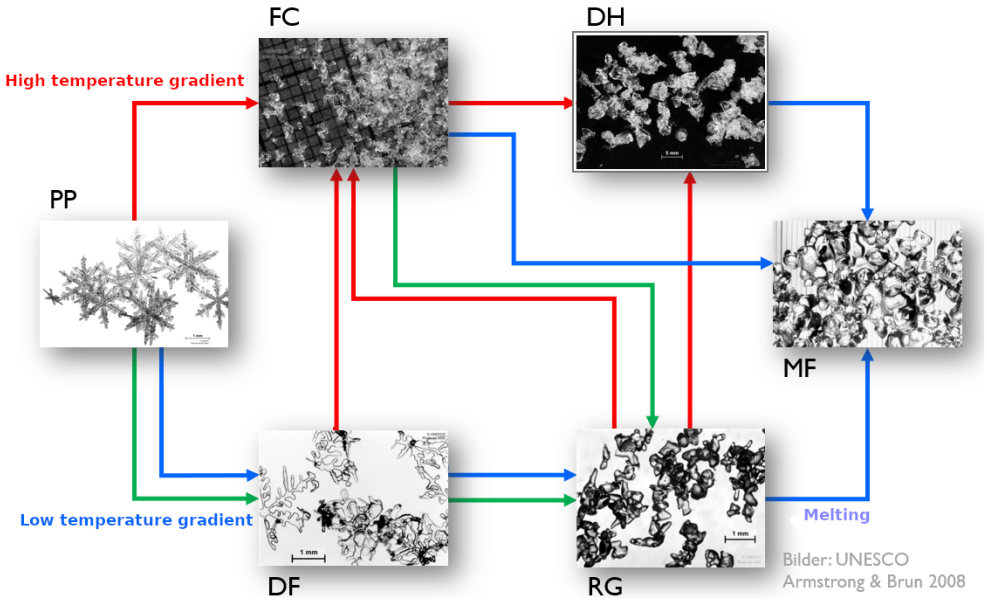

Figure 1: The Snow Metamorphism Process: The green arrows are the rounding processes. Red arrows are the faceting processes. The blue arrows are melting processes. The snow grain types are explained in Table 1.

2.2 Snow Avalanche Formation

A *weak layer* is a layer consisting of snow crystals poorly bonded with the snow layers above and below. There are different kinds of weak layers, consisting of different snow grains (Avalanche Canada [AC], n.d.). The grains have weak bonds and are fragile to external pressure. A weak layer in a snowpack is typically created by the snow metamorphism in the snowpack, as described earlier. If the weak layer resists forming

strong bonds to adjacent layers over a long period, it is called a *persistent weak layer*. Persistent weak layers typically consist of either surface hoar grains, depth hoar grains, or faceted crystals (see Table 1) and can be buried deep in the snowpack (Schweizer et al., 2003).

An avalanche is a rapid motion of snow down a steep slope. They occur in slopes with an angle higher than 30 °. Avalanches can be fatal to human life and also inflicts significant damage on infrastructure. NVE distinguishes between two types of avalanches, loose snow avalanches and slab avalanches (NVE, 2016; Schweizer et al., 2003). A loose snow avalanche is a point-release avalanche, meaning it releases from a point near the snowpack's surface and then spreads down the slope, increasing in volume as it collects snow (Statens Vegvesen, 2014).

Slab avalanches are considered the more dangerous type of avalanche. A bonded layer of snow (called the slab) lies on top of a weak layer. The collapse of the weak layer starts with a minor fracture rapidly propagating through the weak layer. The collapse of a weak layer can either be human-triggered or triggered by natural causes. A human trigger could be an additional load of a skier. A natural trigger could be a large amount of precipitation or wind-drifted snow, leading to rapid changes in the snowpack stratigraphy. In this thesis, the focus is on natural induced slab avalanches. An example of a natural trigger is a large amount of new snow, either as precipitation or drifted by the wind, increasing the stress on the weak layer by the slab above. Figure 2 shows the requirements for the release of a slab avalanche.

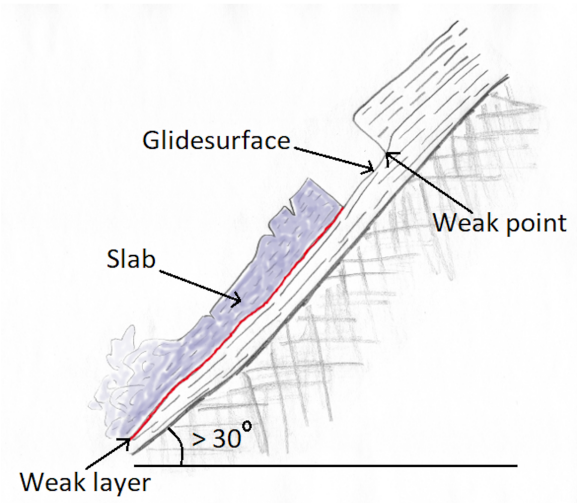

Figure 2: Slab Avalanche: Requirements for a slab avalanche Müller, 2019a.

The formation of a slab avalanche is a complex process depending on interactions within the snowpack, the terrain, and meteorological conditions. Predicting snow avalanches requires an understanding of how different factors impact the stability of the snowpack. *Stability* is the probability that an avalanche will not occur (AAC, n.d.-b). Schweizer et al. (2003) consider five essential factors that contribute to the

stability of a snowpack and, therefore, the avalanche danger: terrain, precipitation (new snow or rain), wind, temperature, and snowpack stratigraphy.

Terrain: An analysis in the Alps, during the winter of 1999, validated that very few avalanches occur when the slope is lower than 30°. There is also evidence that rough terrain or dense forests inhibit avalanche formation, especially if the snow cover has a small depth (< 0.3 m), as snow interception hinders weak layer formation.

Precipitation (New Snow): Accumulation of precipitation, especially as new snow, is critical for avalanche danger, adding weight and therefore stress on the weak layer. Approximately $30 - 50$ cm is considered a critical thickness of new snow depth for naturally released avalanches. The density of new snow also affects the avalanche formation, and a decreasing density with depth is associated with increased avalanche activity.

Wind: Variation in wind speed and wind direction leads to different densities and stress concentrations in the layered snowpack. The snow deposits irregularly, leading to a snowpack with different loading rates.

Temperature: Snow properties are temperature-dependent. Warming temperatures decrease the mechanical hardness of the slab. It also decreases the weak layer's strength and increases the weak layer's toughness. Warm temperatures overall result in a decrease in snowpack stability (Schweizer et al., 2003).

Snowpack stratigraphy: The snowpack properties impact snow avalanche formation and snowpack stability. The weak layer's sheer strength and the grain size and hardness differences between the weak and adjacent layers significantly impact the stability. Snowpack stratigraphy depends on the four other factors listed above as well.

2.3 Stability

An important part of avalanche forecasting, especially for slab avalanches, is stability evaluation. The weak layer stability depends on the ratio between the weak layer strength and the stress put on the weak layer by the overlying slab. Experts manually test the stability with compression tests and hardness tests. Manual tests are time-consuming, requiring people in multiple places in Norway to test the stability every day.

Some metrics have been introduced to measure the stability of a layer quantitatively. Jamieson and Johnston (Jamieson & Johnston, 1998) derived the skier stability index SK_{38}, a quantitative stability measure of a weak layer for a given depth h:

$$\mathrm{SK}_{38} = \frac{\tau}{\tau_{xz} + \Delta\tau_{xz}}, \tag{2.1}$$

where τ is the shear strength per grain type, τ_{xz} being the shear stress due to overlaying slab, and $\Delta\tau_{xz}$ being additional stress induced by a skier.

Snowpack properties such as grain size and hardness are important when evaluating the snowpack's stability, according to Schweizer et al. (2003). As density increases with increasing depth, Schweizer suggested combining SK_{38} with a measure of hardness and grain size difference, resulting in the structural stability index SSI:

$$SSI = SK_{38} + \Delta R^* + \Delta E^*, \tag{2.2}$$

where ΔR^* is the hardness difference across a layer, and ΔE^* the grain size difference across a layer, both taken as binary values, depending on the following formulas:

$$\Delta R^* = \begin{cases} 0 & \text{if } \Delta R \geq 1.5 \\ 1 & \text{if } \Delta R < 1.5, \end{cases} \tag{2.3}$$

$$\Delta E^* = \begin{cases} 0 & \text{if } \Delta E \geq 0.5 \\ 1 & \text{if } \Delta E < 0.5, \end{cases} \tag{2.4}$$

The stability metrics SSI and SK_{38} are both measures of a weak layer's stability. When the stress on the weak layer by the overlying slab, τ_{xz}, increases, the weak layer's stability decreases.

The stability of a weak layer is a highly complex property, depending on numerous combinations of factors. Stability evaluation requires evaluating different information based on equations, observations, and manual stress tests (AAC, n.d.-b). It is therefore not realistic that one equation gives a fully reliable stability measure. Bellaire et al. (2006) showed that both SSI and SK_{38} reproduces reliable stability patterns compared to observed stability patterns. The skier stability index SK_{38} performs well in measuring the stability of a weak layer but poorly locating the weak layer in the snowpack. SSI, on the other hand, performs well in locating the weak layer. A combination of SSI and SK_{38} could therefore indicate the weak layer's stability.

There are few reports on a threshold value of SK_{38} that separates stable and unstable layers. The usual way to determine the stability is by a combination of metrics, for example combining the metrics SSI and SK_{38}. Some report that a layer with a $SK_{38} < 1$ is potentially unstable, while others use a threshold-measure of 0.8 to differentiate the conditions (Monti & Schweizer, 2013; Monti et al., 2014).

2.4 SNOWPACK

SNOWPACK is a numerical snow cover model developed by WSL Institute for Snow and Avalanche Research SLF (SLF, n.d.-c). The model uses differential equations and the finite element method to simulate the snowpack and its development throughout

a chosen period. The main focus is the various processes happening within the snowpack, including detailed information about the evolution of grain size, grain type, density, and hardness of each layer. SNOWPACK calculates a series of layered, one-dimensional snow profiles over a chosen period. With SNOWPACK, it is possible to simulate thin layers if needed, such as an ice crust or a layer consisting of depth hoar grains. Figure 3 shows the different factors impacting the development of a snowpack, which are handled numerically by SNOWPACK. An interesting application of SNOWPACK is that it calculates and outputs the stability of each layer, based on the stability measures SK_{38} and SSI, as described in Chapter 2.3.

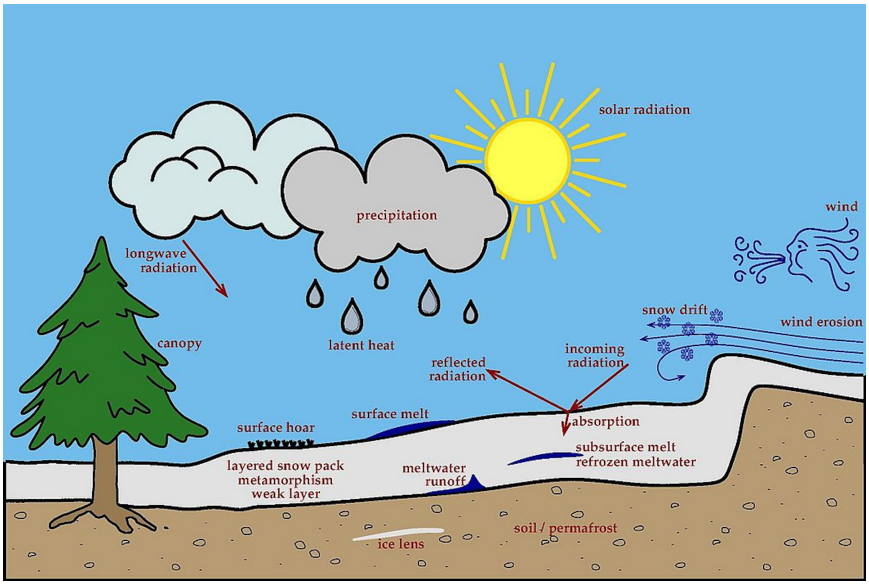

Figure 3: Illustration of the different factors that impacts the development of a snowpack, handled by the numerical snowpack software SNOWPACK (SLF, n.d.-b).

SNOWPACK uses meteorological data from automatic weather stations, predicted weather models, or climate models to simulate the snow cover. Table 2 shows the required inputs to simulate a snow cover model with SNOWPACK. The weather data needs to be at an hourly time-step. To handle missing data, multiple input formats, or damaged data sets, SNOWPACK utilizes a preprocessing library called MeteoIO. MeteoIO preprocesses the data, handles the retrieving, filtering, and resampling of input data, and interpolates data if necessary at the required timestamps. The focus is data quality, with a high emphasis on accuracy and consistency, while obeying the physical laws of nature (Bavay & Egger, 2014).

WxGen is used to generate the meteorological time series data required by SNOWPACK. It is a weather scenarios program developed by the Norwegian Meteorological Institute, which generates and combines weather trajectories stochastically, generating time series of weather within historical trends. The weather trajectories are based on the historical 15-day weather forecast database, ECMWF's (European Centre for Medium-Range Weather Forecasts). WxGen creates gridded time series that are arbi-

Input parameter	Abbrev.
Air temperature	TA
Relative Humidity	RH
Wind speed	WS
Incoming Short Wave Radiation	ISWR
Surface Temperature	TSS
Precipiation	PSUM

Table 2: Weather input required by the numerical snowpack model SNOWPACK.

trarily long, with multiple weather variables. By specifying longitude and latitude, the user can generate weather series at specific locations (MI, n.d.). Figure 4 illustrates the general workflow of producing numerical snowpacks involving WxGen, MeteoIO, and SNOWPACK. Check out the Snowpack and MeteoIO documentation for more specific instructions: https://models.slf.ch/docserver/snowpack/html/getting_started.html.

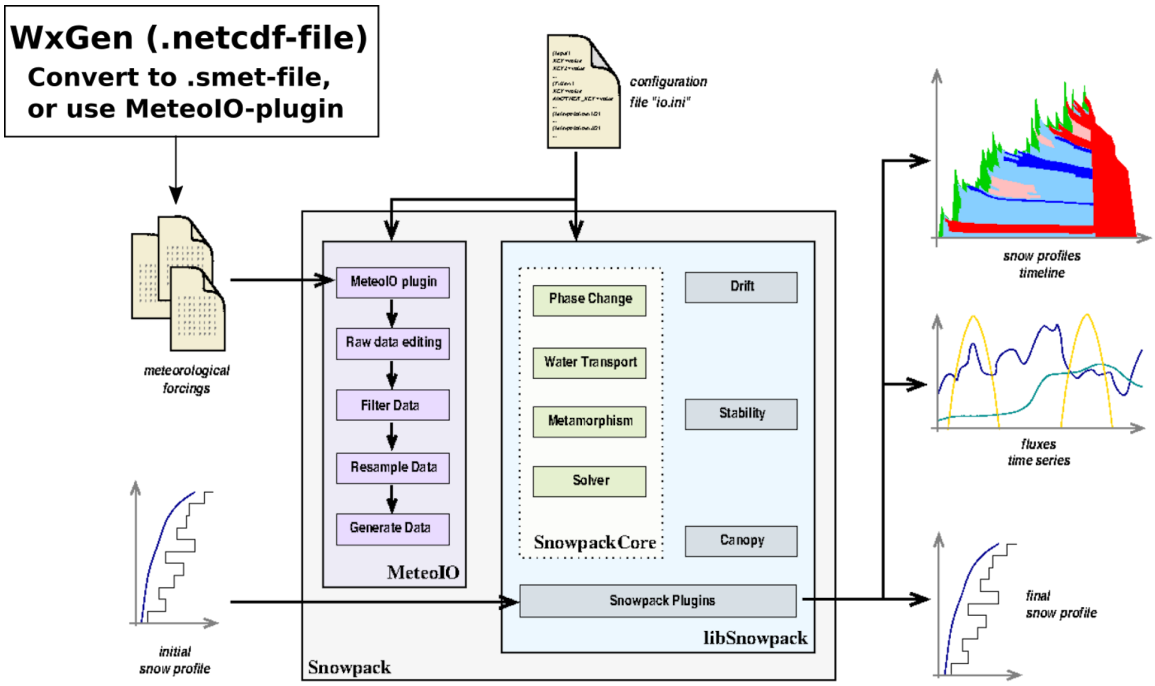

Figure 4: Workflow-illustration of snow cover simulation with WxGen, MeteoIO, SNOWPACK (SLF, n.d.-c).

2.5 Drone Measurement

A developing focus area within snowpack monitoring and avalanche forecasting is the use of Geo-referenced data. An example is the growing use of satellite data, such as the Sentinel satellites, which are part of the Copernicus program by the European Space Agency (ESA). Sentinel satellites make it possible to monitor certain snowpack properties with a spatial resolution of only 10 meters. Data such as snow depth, amount of new snow, and amount of melted snow are continuously monitored and freely available at a website called xGeo[1], developed by NVE (NVE, n.d.).

Another way to provide repeatable and accurate data of a snowpack is by utilizing drone measurements. SINTEF Industry (Applied Geoscience group) launched the GeoDrone project in September 2020, a project that aims to utilize drone measurements to forecast and monitor hazard events such as snow avalanches (Dupuy et al., 2021; SINTEF, n.d.). The project strategy includes building an autonomous and modular drone platform equipped with multi-purpose sensors, including a GPR (Ground Penetrating Radar) for underground mapping and LIDAR/ cameras for surface mapping. Figure 5 displays an outline of the autonomous drone with its measurement functions, and Figure 6 is a picture of the autonomous drone built by SINTEF.

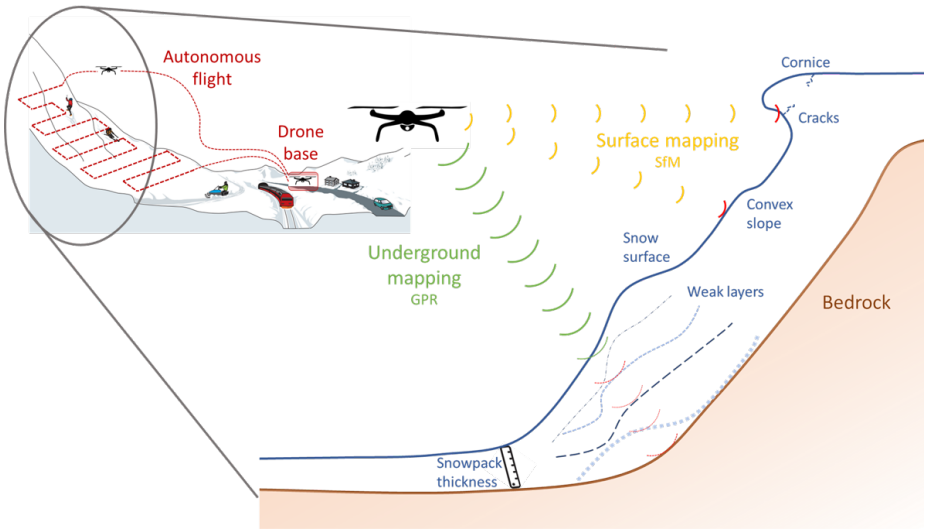

Figure 5: Outline of the autonomous drone with its main functions (Dupuy et al., 2021)

Figure 7 illustrates a simulation of using GPR-data to locate a weak layer in a snowpack. A drone equipped with a GPR emitter sends a signal from 1 m above the snow surface, which propagates down in the snowpack. When the wave meets a layer interface with permittivity contrasts, the signal gets reflected to the GPR emitter, revealing the location and properties of the weak layer in the snowpack. Table 3 lists

[1]http://www.xgeo.no/

Figure 6: Picture of the autonomous drone (Dupuy et al., 2021).

the relative permittivity of each layer in the simulation. The layer of faceted crystals outlined in the figure is considered a weak layer. An ice crust situated on the top of a weak layer is common in a snowpack, as described in Chapter 2.1. Faceted crystals have a low relative permittivity and are therefore difficult to locate using GPR. The ice crust, however, has a high relative permittivity and is observable by the GPR. As the snow below the weak layer is dense, the signal gets reflected, revealing a precise location of the weak layer.

Layer	Relative Permittivity
Air	1
Fresh (New) Snow	1.16
Snow 1	2.1
Ice crust	3.13
Faceted Crystals	1.16
Snow 2	2.5
Depth Hoar	1.16
Bedrock	10

Table 3: The relative permittivity of each layer in the underground-mapping simulation.

SINTEF intends to develop innovative real-time data processing- and data analysis approaches for decision-making to measure the snow properties in real-time. GPR surveys should provide information about layer density and thickness. Surface mapping, using LIDAR or photogrammetry, can also measure the amount of new snow. Grain size and bond size are, at this point, not possible to measure with drones but could be measured by using correlating methods. Such a system must balance the information content of data with the costs of data acquisition and processing. For this purpose, it is useful to build a decision support system that can wisely plan the drone data gathering (Dupuy et al., 2021).

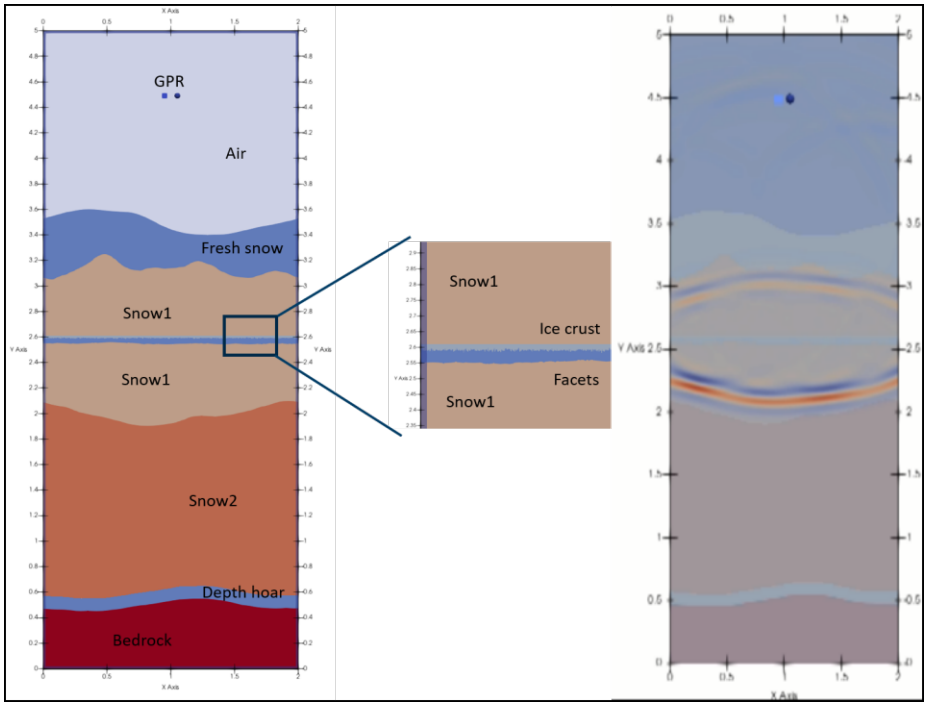

Figure 7: Example of using GPR to locate weak layers in snowpack.

Chapter 3

Modelling Snow Properties

This chapter introduces the first of two stages involved in predicting the stability of the weak layer in a snowpack. The first stage is to forecast the snow properties $X_{t,i}$, where the subscript $t = 1, 2, \ldots$ is the time index, and the subscript $i = 1, 2, \ldots, 6$ is the property index. Table 4 shows the different properties $X_{t,i}$. Properties are estimated daily at 12:00, $t = 1$ indicates day one, $t = 2$ indicates day two etc.

A *Dynamic Linear Model* (DLM) is utilized to capture the effect of time on the snow properties. The second stage is to predict the weak layer stability r_t at time t, using a multivariate regression model with the estimated snow properties $X_{t,i}$ as predictor variables. This stage is presented in Chapter 4. A sequential approach is applied to develop the snowpack properties over time. The model parameters are adjusted depending on the weather conditions at a particular day.

	Variable name:
$X_{t,1}$	New Snow Thickness
$X_{t,2}$	New Snow Density
$X_{t,3}$	Weak Layer Density
$X_{t,4}$	Weak Layer Thickness
$X_{t,5}$	Weak Layer Grain Size
$X_{t,6}$	Weak Layer Bond Size

Table 4: The snow variables used in the dynamic model, at time t.

Chapter 3.1 presents the dynamic model used to forecast the snowpack properties. The conditioning parts of the model ar described in Chapter 3.2.

3.1 Dynamic Model

3.1.1 Developing a model

Let $\mathbf{X}_t = (X_{t,1}, \ldots, X_{t,6})^T$ be a vector containing the snowpack layer properties $X_{t,i}$, at time t. This section develops a model that one-step-forecasts $X_{t,i}$ at any given time t, that is a function $\mathbf{X}_{t+1} = f(\mathbf{X}_t)$. A simple way to calculate $\mathbf{X}_{t+1}$, given $\mathbf{X}_t$ is by a univariate regression model:

$$\mathbf{X}_{t+1} = \boldsymbol{\gamma}_{t+1} + \mathbf{A}_{t+1} \cdot \mathbf{X}_t + \boldsymbol{\epsilon}_{t+1}, \quad \boldsymbol{\epsilon}_{t+1} \sim \mathrm{N}(0, \mathbf{W}_{t+1}), \tag{3.1}$$

where

- $\boldsymbol{\gamma}_{t+1}$ is an (6×1)-vector, containing the intercept at time $t+1$.
- $\mathbf{X}_{t+1}$ is a (6×1)-matrix containing the snow properties at time $t+1$, $\mathbf{X}_t$ similar for time t.
- $\mathbf{A}_{t+1}$ is a (6×6)-diagonal matrix containing the model coefficients, linking each property with itself at the previous time-step, at time $t+1$.
- $\boldsymbol{\epsilon}_{t+1}$ is a (6×1)-vector assumed to be *independent and identically distributed*. $\mathbf{W}_{t+1}$ is the variance of the snowpack properties at time $t+1$.

There is a priori belief that weather has an effect on the development of $X_{t,i}$. By including weather as covariates, the model accommodates this belief. Let $\boldsymbol{\omega}_t$ be a vector containing the weather variables, as listed in Table 5, at time t.

	Variable name:
ω_1	Temperature
ω_2	Precipitation
ω_3	Wind Speed

Table 5: The weather variables used in the dynamic model.

An expansion of Equation 3.1, includes the weather as a factor:

$$\mathbf{X}_{t+1} = \boldsymbol{\gamma}_{t+1} + \mathbf{A}_{t+1} \cdot \mathbf{X}_t + \mathbf{B}_{t+1} \cdot \boldsymbol{\omega}_{t+1} + \boldsymbol{\epsilon}_{t+1}, \tag{3.2}$$

where $\mathbf{B}_{t+1}$ is a $(p \times 3)$-matrix containing the weather-coefficients at time $t+1$ and $\boldsymbol{\omega}_{t+1}$ is a (3×1)-vector containing the weather-data at time $t+1$.

Different weather patterns affect the snow properties in different ways, as described in Chapter 2. There is, therefore, a prior belief that $\mathbf{X}$ develops differently when the external weather patterns change. A combination of temperature, precipitation, and wind speed indicates a weather pattern, further called a *weather regime*. There are eight weather regimes included in the model. Table 6 shows the different weather regimes used in the model.

Regime	Temperature	Precipitation	Wind Speed
HHH	High	High	High
HHL	High	High	Low
HLH	High	Low	High
HLL	High	Low	Low
LHH	Low	High	High
LHL	Low	High	Low
LLH	Low	Low	High
LLL	Low	Low	Low

Table 6: The weather regimes used to group the data in the dynamic model.

The DLM has time-dependent parameters and error terms, depending on the weather regime at a specific day. The parameters $\boldsymbol{\gamma}_{t+1}$, $\mathbf{A}_{t+1}$ and $\mathbf{B}_{t+1}$ all depend on the weather $\boldsymbol{\omega}_{t+1}$ at day $t+1$, and therefore changes according to the regime. The noise term $\boldsymbol{\epsilon}_{t+1}$ also depends on the weather regime at day $t+1$.

3.1.2 Expected Value and Variance

It is important to be able to estimate the mean value and variance of Equation 3.2. Let the expected value $\mathrm{E}(\mathbf{X}_t)$ be denoted as $\hat{\boldsymbol{\mu}}_t$ and the variance $\mathrm{Var}(\mathbf{X}_t)$ at time t be denoted as $\hat{\boldsymbol{\Sigma}}_t$. Then,

$$\begin{aligned}
\hat{\boldsymbol{\mu}}_{t+1} &= \mathrm{E}(\boldsymbol{\gamma}_{t+1} + \mathbf{A}_{t+1} \cdot \mathbf{X}_t + \mathbf{B}_{t+1} \cdot \boldsymbol{\omega}_{t+1} + \boldsymbol{\epsilon}_{t+1}) \\
&= \mathrm{E}(\boldsymbol{\gamma}_{t+1}) + \mathrm{E}(\mathbf{A}_{t+1} \cdot \mathbf{X}_t) + \mathrm{E}(\mathbf{B}_{t+1} \cdot \boldsymbol{\omega}_{t+1}) + \mathrm{E}(\boldsymbol{\epsilon}_{t+1}) \\
&= \boldsymbol{\gamma}_{t+1} + \mathbf{A}_{t+1} \cdot \mathrm{E}(\mathbf{X}_t) + \mathbf{B}_{t+1} \cdot \boldsymbol{\omega}_{t+1} \\
&= \boldsymbol{\gamma}_{t+1} + \mathbf{A}_{t+1} \cdot \hat{\boldsymbol{\mu}}_t + \mathbf{B}_{t+1} \cdot \boldsymbol{\omega}_{t+1}, \qquad (3.3) \\
\hat{\boldsymbol{\Sigma}}_{t+1} &= \mathrm{Var}(\boldsymbol{\gamma}_{t+1} + \mathbf{A}_{t+1} \cdot \mathbf{X}_t + \mathbf{B}_{t+1} \cdot \boldsymbol{\omega}_{t+1} + \boldsymbol{\epsilon}_{t+1}) \\
&= \mathrm{Var}(\boldsymbol{\gamma}_{t+1}) + \mathrm{Var}(\mathbf{A}_{t+1} \cdot \mathbf{X}_t) + \mathrm{Var}(\mathbf{B}_{t+1} \cdot \boldsymbol{\omega}_{t+1}) + \mathrm{Var}(\boldsymbol{\epsilon}_{t+1})) \\
&= \mathbf{A}_{t+1} \hat{\boldsymbol{\Sigma}}_t \mathbf{A}_{t+1}^T + \mathbf{W}_{t+1}. \qquad (3.4)
\end{aligned}$$

3.2 Introduction to a Conditional Model

3.2.1 Information sets

This section introduces sequential modeling, based on the work of West and Harrison (1997). Let $\boldsymbol{\theta}_t$ be the model parameters at time t, the index t indicating that the parameters are dynamic and depends on time. For Equation 3.2, this is given by the set

$$\boldsymbol{\theta}_t = \{\boldsymbol{\gamma}_t, \mathbf{A}_t, \mathbf{B}_t, \boldsymbol{\epsilon}_t\} \qquad (3.5)$$

A DLM has a *sequential* approach, which means that the model focuses on predictive statements of future development, as well as conditioning on existing information.

The information available to a forecaster develops as time evolves. Let D_t be the information available at time t. The initial information available and recognized to a forecaster at $t = 1$ is:

$$D_1 : \textit{initial information set at } t = 1 \tag{3.6}$$

D_1 contains all relevant initial information for forecasting, including the model parameters $\boldsymbol{\theta}_1$ and an initial measurement $\mathbf{X}_1$. For forecasting, the objective is to calculate the forecast distribution $(\mathbf{X}_t|D_1)$, the distribution of $\mathbf{X}_t$ conditional on D_1, where $t > 1$. At time t, denote the information set available as

$$D_t : \textit{information set at time } t \tag{3.7}$$

One-step forecasting to time t involves calculating the forecast distribution $(\mathbf{X}_t|D_{t-1})$, that is the distribution of $\mathbf{X}_t$, conditional on D_{t-1}. The forecast distribution develops with time, updating when new information is available. After observing $\mathbf{X}_t$, the relevant information D_t at time t contains both the previously available information D_{t-1} and the observation $\mathbf{X}_t$. Let I_t be all additional relevant information at time t. This includes the new observations $\mathbf{X}_t$, and possibly revised model parameters at time t, as the parameters are dynamic and depend on the weather regime. Then all the relevant information at time t is

$$D_t = \{I_t,\, D_{t-1}\} \quad t = 1, 2, \ldots \tag{3.8}$$

The sequential approach makes it possible to describe the development of a series by using a probability distribution for $\mathbf{X}_t$, $\mathbf{X}_{t+1}, \ldots$, conditional on past information D_{t-1}. By restricting the model to focus on one-step-predictions, the forecaster's predictive belief is

$$p(\mathbf{X}_t|D_{t-1}, \boldsymbol{\theta}_t), \tag{3.9}$$

where $\boldsymbol{\theta}_t$ is the parameter vector at time t, indicating dynamic parameters, and D_{t-1} is the information set available prior to observing X_t. The predictive density is $p(\mathbf{X}_t|D_{t-1}, \boldsymbol{\theta}_t)$. After observing $\mathbf{X}_t$, the *posterior* distribution is $p(\mathbf{X}_t|D_t)$. The exchange between prior and posterior distribution provides an effective transfer of information through time, making a sequential procedure possible.

3.2.2 Recursive Model

The DLM expressed in Equation 3.2 develops sequentially over time, based on *initializing* the model, *one-step forecasting* the model at time $t + 1$ and *updating* the model distribution given new measurements.

Assume that the property $\mathbf{X}_1$ is known initially, by either some inspection (drone, manual snowpack inspection) or calculated with a numerical model such as SNOWPACK. Then the starting information available at time $t = 1$ is

$$D_1 : \{\mathbf{X}_1,\, \boldsymbol{\theta}_1\} \tag{3.10}$$

where $\boldsymbol{\theta}_1 = \{\mathbf{A}_1, \boldsymbol{\omega}_1, \mathbf{B}_1, \boldsymbol{\gamma}_1\}$ is the parameters at $t = 1$. $(\mathbf{X}_1|D_1)$ is the posterior distribution of $\mathbf{X}_1$, conditional on the available information D_1, at time $t = 1$. The prior distribution $p(\mathbf{X}_2|D_1, \boldsymbol{\theta}_2)$ is calculated by

$$(\mathbf{X}_2|D_1, \boldsymbol{\theta}_2) \sim \mathrm{N}(\hat{\boldsymbol{\mu}}_2, \hat{\boldsymbol{\Sigma}}_2), \tag{3.11}$$

where $\hat{\boldsymbol{\mu}}_2$ and $\hat{\boldsymbol{\Sigma}}_2$ are calculated by Equation 3.3 and Equation 3.4. The posterior distribution at time $t = 2$, after obtaining observation $\mathbf{X}_2$, is $p(\mathbf{X}_2|D_2)$. To separate predicted and updated mean and variance, the following notation is introduced:

- $\hat{\boldsymbol{\mu}}_{t+1|t}$ and $\hat{\boldsymbol{\Sigma}}_{t+1|t}$ is the predicted mean and variance at time $t + 1$, given all the data available at time t, and $\boldsymbol{\theta}_{t+1}$, calculated by equation 3.3 and 3.4.
- $\hat{\boldsymbol{\mu}}_{t+1|t+1}$ and $\hat{\boldsymbol{\Sigma}}_{t+1|t+1}$ is the updated mean and variance at time $t + 1$, given all the data available at time $t + 1$, including measurement $\mathbf{X}_{t+1}$.

The procedure of using posterior, prior, one-step-forecast, and updating the posterior are used recursively for every t, resulting in the sequential model. In general, the recursion follows the three steps:

1. Posterior for $\mathbf{X}_t$: $(\mathbf{X}_t|D_t) \sim \mathrm{N}(\hat{\boldsymbol{\mu}}_{t|t}, \hat{\boldsymbol{\Sigma}}_{t|t})$
2. (One-step forecast) Prior for $\mathbf{X}_{t+1}$: $(\mathbf{X}_{t+1}|D_t, \boldsymbol{\theta}_t) \sim \mathrm{N}(\hat{\boldsymbol{\mu}}_{t+1|t}, \hat{\boldsymbol{\Sigma}}_{t+1|t})$
3. (Update) Posterior for $\mathbf{X}_{t+1}$: $(\mathbf{X}_{t+1}|D_{t+1}) \sim \mathrm{N}(\hat{\boldsymbol{\mu}}_{t+1|t+1}, \hat{\boldsymbol{\Sigma}}_{t+1|t+1})$

Algorithm 1 shows the sequential procedure.

Algorithm 1 Sequential procedure

Inputs:
X_1, A, w, B, γ, T
Output:
X, $\hat{\mu}, \hat{\Sigma}$
Initialize:
$X = [X_1, 0, \dots]$, $\hat{\mu} = [\hat{\mu}_{1|1}, 0, \dots]$, $\hat{\boldsymbol{\Sigma}} = [\hat{\boldsymbol{\Sigma}}_{1|1}, 0, \dots]$, $t = 2$
while $t < T$ **do**
$\hat{\mu}_{t|t-1} \leftarrow \mathrm{E}(X_t)$, $\hat{\Sigma}_{t|t-1} \leftarrow \mathrm{Var}(X_t)$ ▷ using Equation 3.3 and 3.4
$X_t \leftarrow \mathrm{N}(\hat{\mu}_{t|t-1}, \hat{\Sigma}_{t|t-1})$
$X[t] \leftarrow X_t$, $\hat{\mu}[t] \leftarrow \hat{\mu}$, $\hat{\Sigma}[t] \leftarrow \hat{\Sigma}$
$t \leftarrow t + 1$
end while

Chapter 4

Drone Assimilation and Adaptive Monitoring

The second stage of the model concerns predicting the weak layer stability r_t, based on the estimated snow properties $\mathbf{X}_t$. Chapter 2.2 describes how the weak layer stability depends on both weak layer properties and new snow layer properties. A multivariate regression model is proposed:

$$r_t = \mathbf{f} \cdot \mathbf{X_t} + \tau_t, \quad \tau_t \sim \mathrm{N}(0, V_t), \tag{4.1}$$

where $\mathbf{f}$ is a $(1 \times p)$-coefficient matrix constant for all t, and τ_t is the associated error of the predicted stability at time t, assumed to be normal distributed with variance V_t.

4.1 Threshold test

For each day t, the model predicts the weak layer stability r_t, based on the one-step-forecasted snow properties $\mathbf{X}_t$ as calculated in Equation 3.2. Assume at a time t, the expected value and variance of $\mathbf{X}_{t+1}$ are estimated as $\hat{\boldsymbol{\mu}}_{t+1|t}$ and $\hat{\boldsymbol{\Sigma}}_{t+1|t}$ respectively, using the sequential procedure introduced in Chapter 3.2. At time t, the available data is the information set D_t. Using equation 4.1, the model calculates

$$r_{t+1}|D_t \sim (\hat{f}_{t+1|t}, \hat{Q}_{t+1|t}), \tag{4.2}$$

where

$$\hat{f}_{t+1|t} = \mathbf{f} \cdot \hat{\boldsymbol{\mu}}_{t+1|t} \tag{4.3}$$

$$\hat{Q}_{t+1|t} = \mathbf{f}^T \hat{\boldsymbol{\Sigma}}_{t+1|t} \mathbf{f} + V_{t+1}. \tag{4.4}$$

The goal is to subject the estimated stability to a threshold test. Let the *Estimated Stability Threshold*, further denoted as EST, be the lowest possible stability measure

before a weak layer is deemed potentially unstable. The prior probability that the predicted stability at time $t+1$ is higher than EST is given by

$$p = P(r_{t+1} \geq \text{EST}|D_t) = P(-r_{t+1} \leq \text{EST}|D_t) = P\left(Z \leq \frac{\hat{f}_{t+1|t} - \text{EST}}{\sqrt{\hat{Q}_{t+1|t}}}\right). \quad (4.5)$$

That is the probability that the predicted stability is higher than the EST given information D_t.

4.2 Updating with drone measurements:

The model is further developed to update the model distribution with drone measurements. Using the Bayesian framework, the model updates its posterior distribution based on drone measurements $\mathbf{d}_t$. The equations for the updated drone measurements is given by

$$\mathbf{d}_{t+1} = \mathbf{G} \cdot \mathbf{X}_{t+1} + \boldsymbol{\delta}_{t+1},\ \boldsymbol{\delta}_{t+1} \sim \text{N}(0, \mathbf{R}_{t+1}), \quad (4.6)$$

where $\mathbf{X}_{t+1} \sim \text{N}(\hat{\boldsymbol{\mu}}_{t+1|t}, \hat{\boldsymbol{\Sigma}}_{t+1|t})$ and $\mathbf{R}_{t+1}$ is the variance accociated with the drone. The updated posterior distribution after receiving a drone measurement is calculated by

$$\mathbf{X}_{t+1}|D_{t+1} \sim \text{N}(\hat{\boldsymbol{\mu}}_{t+1|t+1}, \hat{\boldsymbol{\Sigma}}_{t+1|t+1}), \quad (4.7)$$

where

$$\hat{\boldsymbol{\mu}}_{t+1|t+1} = \hat{\boldsymbol{\mu}}_{t+1|t} + \hat{\boldsymbol{\Sigma}}_{t+1|t}\mathbf{G}^T \cdot [\mathbf{G}\hat{\boldsymbol{\Sigma}}_{t+1|t}\mathbf{G}^T + \mathbf{R}_{t+1}]^{-1} \cdot (\mathbf{d}_{t+1} - \mathbf{G}\boldsymbol{\mu}_{t+1|t}), \quad (4.8)$$

$$\hat{\boldsymbol{\Sigma}}_{t+1|t+1} = \hat{\boldsymbol{\Sigma}}_{t+1|t} - \underbrace{\hat{\boldsymbol{\Sigma}}_{t+1|t}\mathbf{G}^T[\mathbf{G}\hat{\boldsymbol{\Sigma}}_{t+1|t}\mathbf{G}^T + \mathbf{R}_{t+1}]^{-1}\mathbf{G}\hat{\boldsymbol{\Sigma}}_{t+1|t}}_{\mathbf{S}_{t+1}}. \quad (4.9)$$

The updated stability r_{t+1} after a drone measurement is calculated by

$$\text{E}(r_{t+1}|D_t, \mathbf{d}_{t+1}) = \hat{f}_{t+1|t+1} = \mathbf{f} \cdot \hat{\boldsymbol{\mu}}_{t+1|t+1}, \quad (4.10)$$

$$\text{Var}(r_{t+1}|D_t, \mathbf{d}_{t+1}) = \hat{Q}_{t+1|t+1} = \mathbf{f}^T\hat{\boldsymbol{\Sigma}}_{t+1|t+1}, \mathbf{f} + V_{t+1} \quad (4.11)$$

Then the updated stability is calculated by

$$(r_{t+1}|D_t, \mathbf{d}_{t+1}) \sim \text{N}(\hat{f}_{t+1|t+1}, \hat{Q}_{t+1|t+1}). \quad (4.12)$$

4.3 Adaptive Monitoring Strategy

This section presents an adaptive monitoring strategy useful for deciding when to initiate drone events. The strategy is based on standard event-based decision strategies, as described by Shi, Shi, and Chen (2016). This section introduces the **Adaptive Monitoring (AMA)** strategy. With the AMA strategy, the model updates with either drone-measured properties $\mathbf{d}_{t+1}$ or the estimated properties $\mathbf{X}_{t+1}$, depending on the predicted stability. The AMA strategy is structured the following way:

- Predict the probability p that the predicted weak layer stability is higher than EST.
- If the probability p is lower than a threshold L, monitor snowpack with drone, obtain drone measurement $\mathbf{d}_{t+1}$
- Update model with drone data $\mathbf{d}_{t+1}$, so posterior distribution is $p(\mathbf{X}_{t+1}|D_{t-1}, \mathbf{d}_{t+1})$

Let L be a probability threshold, indicating the probability required to start a drone event. Then for time t the following decision rule is given

- $p > L$: Do not inspect snowpack-properties with drone.
- $p \leq L$: Inspect snowpack-properties with drone.

The extended model using the AMA strategy are summarised by the following equations.

$$r_{t+1} = \mathbf{f} \cdot \mathbf{X}_{t+1} + \tau_{t+1}, \quad \tau_{t+1} \sim \mathrm{N}(\mathbf{0}, Q_{t+1}) \tag{4.13}$$

$$\mathbf{X}_{t+1} = \mathbf{A}_{t+1} \cdot \mathbf{X}_t + \mathbf{B}_{t+1} \cdot \boldsymbol{\omega}_{t+1} + \boldsymbol{\epsilon}_{t+1}, \quad \boldsymbol{\epsilon}_{t+1} \sim \mathrm{N}(\mathbf{0}, \mathbf{W}_{t+1}) \tag{4.14}$$

Below is an outline of a sequential procedure incorporating the dynamic part of Equation 4.14 and the stability part of Equation 4.13. The procedure is inspired by the work of West and Harrison concerning sequential procedures for DLM's (West & Harrison, 1997). a) and b) describes the first stage of the procedure (forecasting), while c) and d) describes the second stage of the procedure (updating).

First, the model uses the prior distribution, based on the available information at time t, to forecast $\mathbf{X}_{t+1}$. Then the model predicts the stability measure r_{t+1} and calculates the probability p that the predicted stability is higher than EST. If the probability is less than a probability threshold L, a drone is initiated to measure the snow properties. The model uses the new measurement (either a drone mesasurement or X_{t+1} depending on the result of the decision rule) to update the posterior distribution for $t + 1$. The following notation is introduced to separate if the updated distribution uses a drone measurement or an estimated snow property:

- $\boldsymbol{\mu}_{t+1|t+1}$ and $\boldsymbol{\Sigma}_{t+1|t+1}$ means mean and variance given data available at time $t + 1$, when updated with estimated properties.
- $\boldsymbol{\mu}_{t+1|0}$ and $\boldsymbol{\Sigma}_{t+1|0}$ means mean and variance given data available at time $t + 1$, when updated with drone measurements.

Sequential Procedure:

a) Posterior at time t:
Given information set D_t, with some known mean $\hat{\boldsymbol{\mu}}_t$ and variance $\hat{\boldsymbol{\Sigma}}_t$.

$$(\mathbf{X}_t|D_t) \sim \mathrm{N}(\hat{\boldsymbol{\mu}}_{t|t},\, \hat{\boldsymbol{\Sigma}}_{t|t}). \tag{4.15}$$

b) Prior for time $t+1$:
Let $\hat{\boldsymbol{\mu}}_{t+1|t} = \mathbf{A}_{t+1}\hat{\boldsymbol{\mu}}_{t|t} + \mathbf{B}_{t+1}\boldsymbol{\omega}_{t+1}$ and $\hat{\boldsymbol{\Sigma}}_{t+1|t} = \mathbf{A}_{t+1} \cdot \boldsymbol{\Sigma}_{t|t}{\mathbf{A}_{t+1}}^T + \mathbf{W}^{t+1}$, estimated by Equation 3.3 and Equation 3.4 respectively. Then

$$(\mathbf{X}_{t+1}|D_t, \boldsymbol{\theta}_{t+1}) \sim N(\hat{\boldsymbol{\mu}}_{t+1|t},\, \hat{\boldsymbol{\Sigma}}_{t+1|t}). \tag{4.16}$$

c) One-step forecast (Event trigger):
Let $\hat{f}_{t+1|t} = \mathbf{f}\hat{\boldsymbol{\mu}}_{t+1|t}$ and $\hat{Q}_{t+1|t} = \mathbf{f}^T\hat{\boldsymbol{\Sigma}}_{t+1|t}\mathbf{f} + V_{t+1}$, estimated by Equation 4.3 and Equation 4.4 respectively. Then

$$(r_{t+1}|D_t, \boldsymbol{\theta}_{t+1}) \sim \mathrm{N}(\hat{f}_{t+1|t},\, \hat{Q}_{t+1|t}). \tag{4.17}$$

d) Posterior at $t+1$ (Updating):
If $p(r_{t+1} \geq \mathrm{EST}|D_t, \boldsymbol{\theta}_{t+1}) > L$: Let D_{t+1} be the updated information set for $t+1$, containing the predicted mean and variance, as estimated earlier: $\hat{\boldsymbol{\mu}}_{t+1|t+1} = \hat{\boldsymbol{\mu}}_{t+1|t}$ and $\hat{\boldsymbol{\Sigma}}_{t+1|t+1} = \hat{\boldsymbol{\Sigma}}_{t+1|t}$.

$$(\mathbf{X}_{t+1}|D_{t+1}) \sim \mathrm{N}(\hat{\boldsymbol{\mu}}_{t+1|t+1},\, \hat{\boldsymbol{\Sigma}}_{t+1|t+1}). \tag{4.18}$$

If $p(r_{t+1} \geq \mathrm{EST}|D_t, \boldsymbol{\theta}_{t+1}) \leq L$: Let $\bar{D}_{t+1}$ be the updated information set for $t+1$, containing the drone-measurements given by equation 4.7. The variance $\boldsymbol{\Sigma}_{t+1|0}$ depends on the drone resolution. If there are missing drone-data, the model uses the estimated properties for the specific variables.

$$(\mathbf{X}_{t+1}|\bar{D}_{t+1}) \sim N(\boldsymbol{\mu}_{t+1|0},\, \boldsymbol{\Sigma}_{t+1|0}). \tag{4.19}$$

As the model develops over time, the variance propagates, yielding more uncertain forecasts. Inspecting the snowpack properties with a drone should give more accurate measurements than estimation by the dynamic model, especially at higher t-values. Thus, an adaptive model that updates its distribution based on drone measurements should provide more reliable results than a non-adaptive model. The determination of the EST value is important in this regard, as it impacts when the model initiates a drone. Figure 8 shows the model workflow, and Algorithm 2 is the pseudocode for the DLM using the AMA strategy.

Algorithm 2 AMA-Algorithm

Inputs:
L, EST, T, F, X_1, A, ω, B, γ
Output:
X, r
Initialize:
$r \leftarrow [0, \dots]$
$X = [X_1, 0, \dots]$
$D = \emptyset$
while $t < T$ **do**
X_t, $\hat{\boldsymbol{\mu}}_t$, $\hat{\boldsymbol{\Sigma}}_t \leftarrow$ Sequential Procedure$(X_{t-1}, A, w, B, \gamma, T)[t]$ ▷ See Algorithm 1
$\hat{f}_t \leftarrow \mathrm{E}[r_t|D]$, $\hat{Q} \leftarrow \mathrm{Var}[r_t|D]$ ▷ See Equation 4.3 and 4.4
$r_t \leftarrow \mathrm{N}(\hat{f}_t, \hat{Q}_t)$
$r[t] \leftarrow r_t$
$p \leftarrow P(r_t \geq \mathbf{EST})$
if $p \leq L$ **then**
Inspect with drone, obtain measured snowpack properties d_t
$X[t] \leftarrow d_t$
$D = D \cup d_t$
else
Use estimated snowpack properties X_t
$X[t] \leftarrow X_t$
$D = D$
end if
Update distribution $P(X_t) = P(X_t|D)$
t=t+1
end while

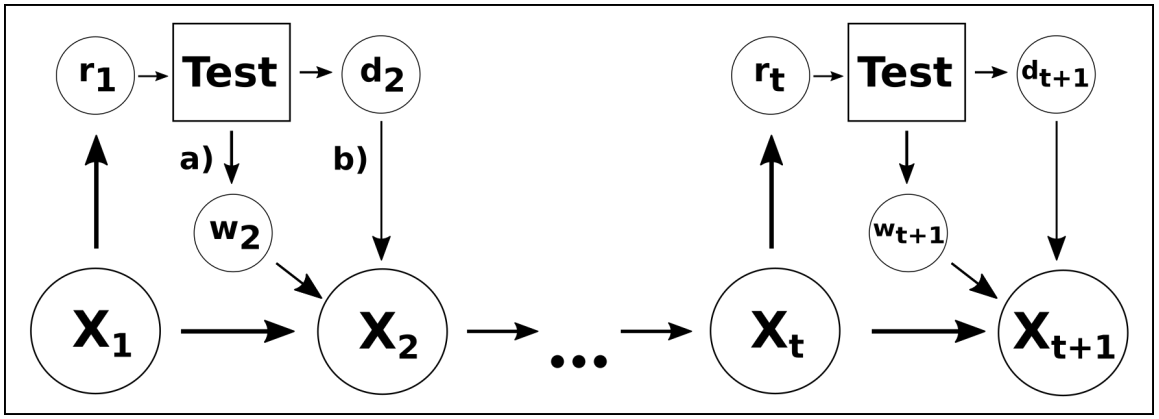

Figure 8: The workflow of the dynamic model. Test is the threshold-test, that either uses the estimated properties dependent on weather-data or a drone-measurement in the next iteration.

4.4 Value of Information Strategy

Another strategy to initiate drones is using **Value of Information (VOI)**. VOI is a useful way to quantify the value of a drone measurement before it is acquired. With a VOI strategy, the goal is to use the expected value of information in a drone measurement to decide if a drone should be initiated. Eidsvik et al. (2015) describe three relevant conditions that affect the value of information, contained into the *pyramid of conditions*:

1. Relevancy: Is the information relevant to the value?
2. Material: Can the information change the decision?
3. Economic: Is the value of information higher than the cost of the information?

Assume there is a high probability that an avalanche occurs and blocks the road if the predicted weak layer stability is less than EST. Discussion around the validity of using a single stability prediction to predict avalanches is discussed in Chapter 7. There are two actions available, either close the road or keep the road open and risk that the stability is lower than the stability threshold:

- **Alternative 1**: Close road
- **Alternative 2**: Keep road open

With a VOI-strategy, it is possible to find the expected cost of each alternative given an unobserved drone measurement. It can therefore be used as a decision rule, by choosing the cheapest alternative every day. Closing the road will naturally have a higher cost than keeping the road open, as closing roads stops traffic. Let C_0 be the cost of closing the road. The expected cost of alternative 2 however depends on

the probability $P(r_{t+1} \leq \text{EST})$, that is the probability that the predicted weak layer stability is less than the threshold EST. C_1 is the cost associated with a blocked road. The expected cost of alternative 2 is then $C_1 \cdot P(r_{t+1} \leq \text{EST})$. The *Prior Value* (PV) is given by

$$\text{PV} = \min\{C_0, C_1 \cdot P(r_{t+1} \leq \text{EST}|D_t))\} \tag{4.20}$$

$$= \min\left\{C_0, C_1 \cdot \Phi\left(\frac{\text{EST} - \hat{\mathbf{f}}}{\sqrt{\hat{\mathbf{Q}}_{t+1|t}}}\right)\right\} \tag{4.21}$$

The next step is to assume a drone has obtained new data $\mathbf{d}_{t+1}$. The *Posterior Value* (PoV) is

$$\text{PoV}(\mathbf{d}_{t+1}) = \min\{C_0, C_1 \cdot P(r_{t+1} \leq \text{EST}|D_t, \mathbf{d}_{t+1}))\} \tag{4.22}$$

The Value of Information is defined as the expected gain in value

$$\text{VOI}(\mathbf{d}_{t+1}) = \text{E}[\text{PoV}(\mathbf{d}_{t+1})] - \text{PV} \tag{4.23}$$

$\text{VOI}(\mathbf{d}_{t+1})$ measures how valueable the drone measurement $\mathbf{d}_{t+1}$ is to the belief of r_{t+1}. Large $\text{VoI}(\mathbf{d}_{t+1})$-values indicates that the measured properties has a large impact on the belief about r_{t+1}. The expected PoV of a drone measurement is given by

$$\text{E}[\text{PoV}(\mathbf{d}_{t+1})] = \int \min\{C_0, C_1 \cdot P(r_{t+1} \leq \text{EST}|D_t, \mathbf{d}_{t+1}))\} \cdot p(\mathbf{d}_{t+1}|D_t)\mathbf{d}_{t+1}, \tag{4.24}$$

$$= \int \min\left\{C_0, C_1 \cdot \Phi\left(\frac{\text{EST} - \mathbf{f} \cdot \hat{\boldsymbol{\mu}}_{t+1|t+1}}{\sqrt{\hat{\mathbf{Q}}_{t+1|t+1}}}\right)\right\} \cdot p(\mathbf{d}_{t+1}|D_t)\mathbf{d}_{t+1}, \tag{4.25}$$

$$= \int \min\{C_0, C_1 \cdot \Phi(w)\} \cdot p(w)d_w, \tag{4.26}$$

where

$$w = \frac{\text{EST} - \mathbf{f} \cdot \hat{\boldsymbol{\mu}}_{t+1|t+1}}{\sqrt{\hat{Q}_{t+1|t+1}}}, \tag{4.27}$$

The expected value and variance of w given the information D_t is given by

$$\text{E}(w|D_t) = \mu_w = \frac{\text{EST} - \mathbf{f} \cdot \hat{\boldsymbol{\mu}}_{t+1|t}}{\sqrt{\hat{\mathbf{Q}}_{t+1|t+1}}} \tag{4.28}$$

$$\text{Var}(w|D_t) = \sigma_w^2 = \frac{\mathbf{f} \cdot \mathbf{S}_{t+1} \cdot \mathbf{f}^T}{\hat{\mathbf{Q}}_{t+1|t+1}}, \tag{4.29}$$

where $\mathbf{S}_{t+1}$ is given by equation 4.9. Let

$$w^* = \Phi^{-1}\left(\frac{C_0}{C_1}\right) \tag{4.30}$$

The extension of Equation 4.26 is given by

$$\mathrm{E}[\mathrm{PoV}(\mathbf{d}_{t+1})] = C_0 \int_{w^*}^{\infty} p(w) d_w + C_1 \int_{-\infty}^{w^*} \Phi(w) \cdot p(w) \cdot d_w \tag{4.31}$$

$$= C_0 \left[1 - \Phi\left(\frac{w^* - \mu_w}{\sigma_w} \right) \right] + C_1 \cdot P(Z < W, W < w^*), \tag{4.32}$$

Let now

$$Z_1 = \frac{Z - W - (0 - \mu_w)}{\sqrt{1 + \sigma_w^2}} \sim \mathrm{N}(0, 1) \tag{4.33}$$

$$Z_2 = \frac{W - w^* - (\mu_w - w^*)}{\sigma_w} \sim \mathrm{N}(0, 1), \tag{4.34}$$

The covariance between Z_1 and Z_2 is given by

$$\delta = \mathrm{Cov}(Z_1, Z_2) = \mathrm{Cov}\left(-\frac{w}{\sqrt{1 + \sigma_w^2}}, \frac{w}{\sigma_w} \right) \tag{4.35}$$

$$= -\frac{1}{\sigma_w \sqrt{1 + \sigma_w^2}} \cdot \mathrm{Var}(w) = -\frac{\sigma_w}{\sqrt{1 + \sigma_w^2}} \tag{4.36}$$

Define that

$$a_1 = \frac{\mu_w}{\sqrt{1 + \sigma_w^2}} \tag{4.37}$$

$$a_2 = \frac{w^* - \mu_w}{\sigma_w} \tag{4.38}$$

The expected PoV is then given by

$$\mathrm{E}[\mathrm{PoV}(\mathbf{d}_{t+1})] = C_0 \Phi\left(\frac{\mu_w - w^*}{\sigma_w} \right) + C_1 \Phi_2\left(\begin{pmatrix} a_1 \\ a_2 \end{pmatrix}; \begin{pmatrix} 0 \\ 0 \end{pmatrix}, \begin{pmatrix} 1 & \delta \\ \delta & 1 \end{pmatrix} \right), \tag{4.39}$$

where Φ_2 is the bivariate cumulative distribution function. The expected VOI of an observation $\mathbf{d}_{t+1}$ is then given by

$$\mathrm{E}[\mathrm{VOI}(\mathbf{d}_{t+1})] = \mathrm{E}[\mathrm{PoV}(\mathbf{d}_{t+1})] - \mathrm{PV} \tag{4.40}$$

This expected value can be used as a criteria to decide if a drone-inspection is needed. Finally, the criteria is subjected to the threshold value L_{VOI}, using the following decision rule:

$$\mathrm{E}[\mathrm{VOI}(\mathbf{d}_{t+1})] \geq L_{\mathrm{VOI}} \implies \text{Gather data with drone} \tag{4.41}$$

$$\mathrm{E}[\mathrm{VOI}(\mathbf{d}_{t+1})] < L_{\mathrm{VOI}} \implies \text{Do not gather data with drone} \tag{4.42}$$

Some important considerations need to be taken into account with a VOI-strategy model. The parameters L_{VOI}, EST, C_0 and C_1 all impact when the drone is initiated and needs to be determined carefully. For example, if the cost of C_0 and C_1 is close, there would be less gained by obtaining a drone measurement, as it has less financial significance to send out a drone. If the cost C_1 is much higher than C_0, however, there is more value to a drone measurement, as the cost associated with predicting stability lower than the threshold is higher.

Algorithm 3 Information-based-monitoring

Inputs:
L_{VOI}, EST, T,X_1, A, ω, B, γ, C_0, C_1
Output:
X, r
Initialize:
$r \leftarrow [0, \dots]$
$X = [X_1, 0, \dots]$
$D = \emptyset$
while $t < T$ **do**
X_t, $\hat{\boldsymbol{\mu}}_t$, $\hat{\boldsymbol{\Sigma}}_t \leftarrow$ Sequential Procedure$(X_{t-1}, A, w, B, \gamma, T)[t]$ ▷ See Algorithm 1
$\hat{f} \leftarrow \text{E}[r_t|D]$, $\hat{Q} \leftarrow \text{Var}[r_t|D]$ ▷ See Equation 4.3 and 4.4
$r_t \leftarrow \text{N}(\hat{f}, \hat{Q})$
Calculate E[PoV(d_{t+1})] with Equation 4.39
E[VOI(d_t)] $\leftarrow$ E[PoV(d_t)] $- PV$
if E[VOI(d_t)] $\geq L_{\text{VOI}}$ **then**
Inspect with drone, obtain measured snowpack properties d_t
$X[t] \leftarrow d_t$
$D \leftarrow D \cup d_t$
else
Use estimated snowpack properties X_t
$X[t] \leftarrow X_t$
$D \leftarrow D$
end if
Update distribution $P(X_t) = P(X_t|D)$
$t = t + 1$
end while

Chapter 5

Generating Data

This chapter presents the data used in the analysis in Chapter 6. Chapter 5.1 introduces the general study area. The generated weather scenarios and the simulated snowpacks are presented in Chapter 5.2. Chapter 5.3 presents the snow properties and the stability measures calculated by SNOWPACK. Finally, Chapter 5.4 describes the grouping of data into weather regimes. The code used to extract and generate the data described in this chapter are included in Appendix B.

5.1 Study Area

The chosen Study Area is Stryn, a municipality in Vestland county, in the western part of Norway, alongside the national road from Lom to Stryn (Riksvei 15). The road passes the mountain range Strynefjellet, an avalanche-prone area with frequent strong winds. It is the fastest road between Nordfjord and Indre Østlandet, the fastest winter road between Vestlandet and Trøndelag, and a popular tourist road connecting the southern mountain ranges with the fjords in Nordfjord and Sunnmøre. Two locations in Stryn are included in the data set: **Kroken** and **Fjellet**. Kroken is the name of a weather station operated by the Norwegian Meteorological Institute. Fjellet is a shortening of the name Strynefjell-Kvitenova, and is a weather station operated by The Norwegian Public Roads Administration. Figure 9 shows the two weather stations alongside Riksvei 15. Kroken is around 200 meters above sea level, while Fjellet is situated higher in the mountain, at around 1000 meters above sea level.

5.2 Wxgen and Snowpack data

Figure 10 shows the generated weather sequences of four different weather variables at Kroken and Fjellet in Stryn, generated with WxGen (see a description of WxGen in Chapter 2.4). The simulation period of weather scenarios is between January 1 and April 30. The geographical closeness between Kroken and Fjellet explains the apparent correlation for each weather variable.

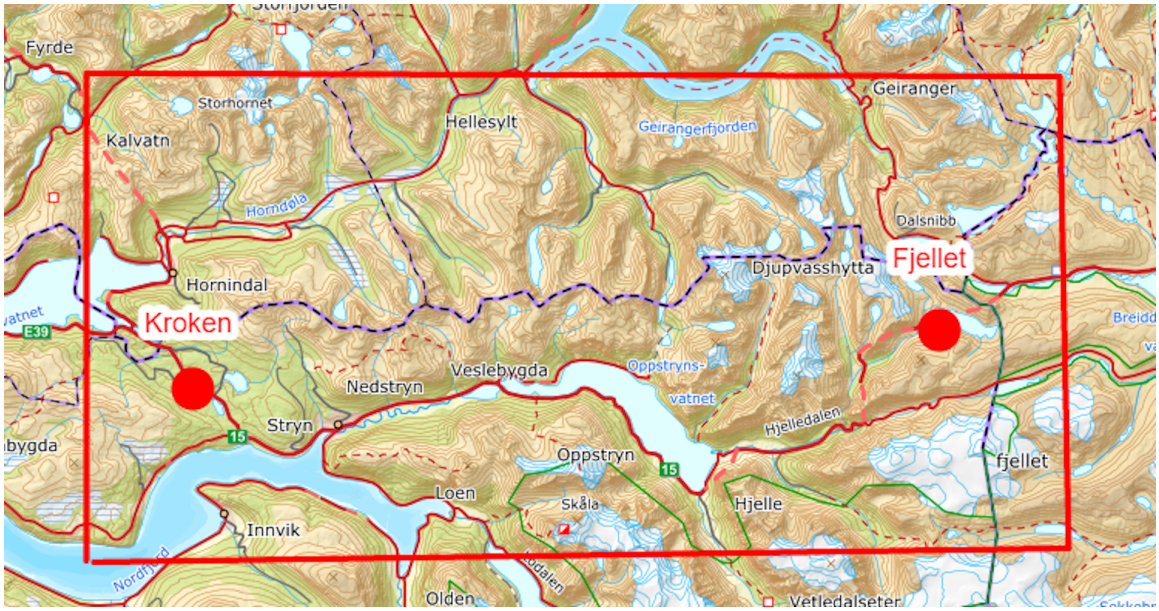

Figure 9: The study area in Stryn, with the two weather stations Kroken and Fjellet included.

The average temperature varies a lot every day but has an overall rising trend, as expected in the spring. There are some indications of a seasonal trend, with consecutive days of either cold temperatures or warm temperatures. The precipitation graph shows that January and late March (and onwards) were the driest periods. There is also an apparent wet period from the middle of February to the beginning of March with consecutive days with a large amount of precipitation. The wind speed varies a lot over the whole period. The average wind speed is higher in January, February, and the beginning of March than in the later periods. The incoming solar radiation rises over the spring, as expected due to the seasonal change. The trends described supports the idea of grouping data into weather regimes, which are described further in Chapter 5.4.

The weather sequences provide input for the numerical model SNOWPACK (see further details on SNOWPACK in Chapter 2.4). Figure 11 shows the simulated snowpacks at Kroken (a) and Fjellet (b). The colors correspond to the grain type of each snowpack layer (see further descriptions about the different grain types in Chapter 2.1). The light blue layers consist of faceted crystals, the dark blue layers consist of depth hoar crystals, and the light green layers consist of new snow grain types. These three layers are the main focus of this thesis, as weak layers often consist of depth hoar or faceted crystals, and new snow adds to the load on the weak layer, affecting its stability. See more on the different factors affecting weak layer stability in Chapter 2.2.

The similarities between the simulated snowpacks at Kroken and Fjellet result from similarities in the generated weather sequences at the two locations. The snowpack at Fjellet has a higher snow height than at Kroken during most of the winter. The

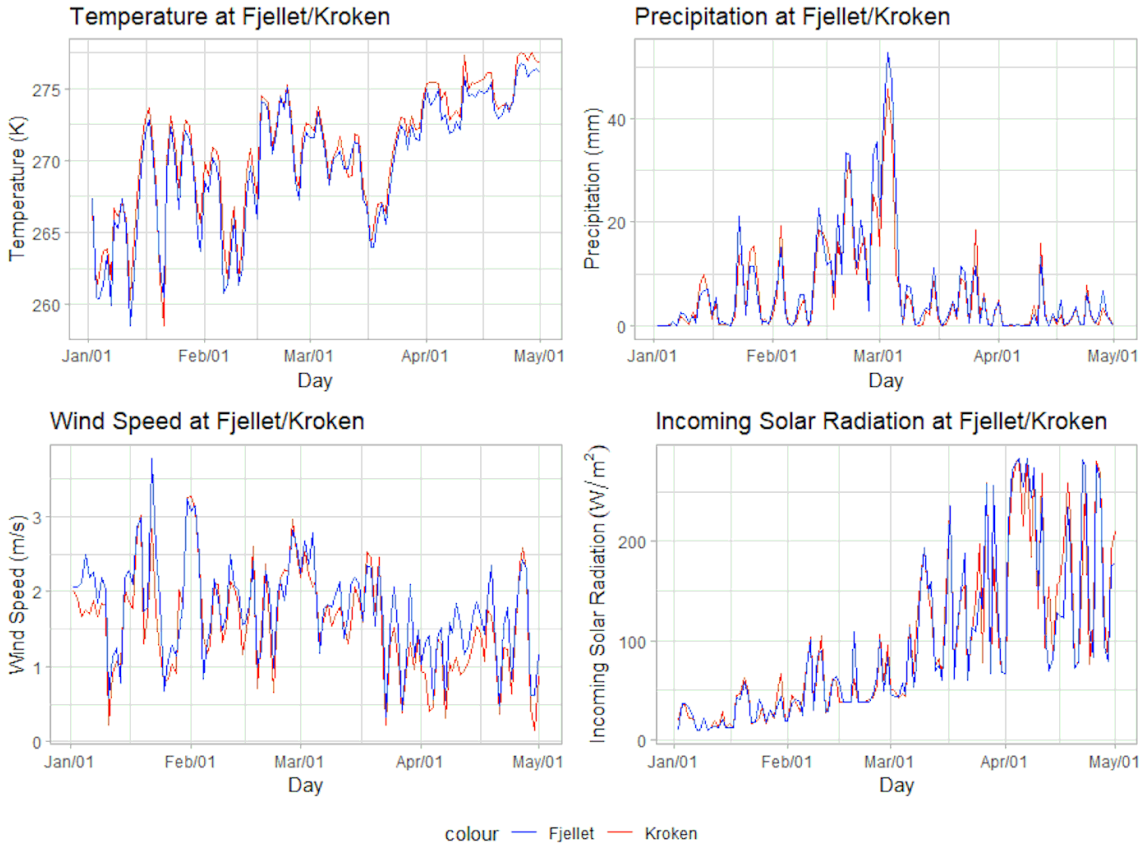

Figure 10: Simulated weather scenarios at Fjellet (blue color) and Kroken (red color) from January 1 to April 30.

difference in snow height is most likely due to Fjellet being situated at a higher altitude than Kroken and therefore exposed to a harsher climate.

Two important outputs of SNOWPACK are the mechanical stability measures SSI and SK_{38} of each layer in the snowpack. SSI and SK_{38} are described in Chapter 2.3. SSI is used to determine the snowpack's weakest layer, as the layer with the lowest SSI, is determined as the weakest layer. The weakest layer changed between multiple layers during the simulation period. To focus on one layer, the layer that most frequently had the lowest SSI was determined as the snowpack's weakest layer. As this layer was prominent over the whole winter period, it is denoted as a persistent weak layer. SNOWPACK also provides the other stability output SK_{38}. The determination of which stability measure to use as the response when predicting the stability is done in Chapter 6.

5.3 New Snow and Weak Layer properties

Figure 12 shows the new snow layer and weak layer properties at both Kroken and Fjellet as time series from January 18 to April 16. SNOWPACK was first able to produce reliable stability output from January 18, as the snowpack was too small and undeveloped before that. The change of end date happened because a majority of the snow had turned into melting forms in the middle of April due to high temperatures and a high amount of incoming solar radiation (see Figure 10). This lead to an absence of new snow grains, which is one of the main focus areas in this project. The end date was therefore pushed to April 16.

Notice in Figure 12 that the thickness of the new snow is highest in February. February is a period with cold weather and a moderately high amount of precipitation, resulting in a rapid build-up of snow height. The thickness of new snow decreases sharply in March. While March has the highest amount of precipitation over the whole period, it is also a much warmer month. Warm temperatures cause a rounding effect on the snow grains, turning the new snow grains into rounded grains, as described in Chapter 2.1. The new snow density varies around 100 kg/m^3, with some outliers reaching 300 kg/m^3. The density necessarily decreases to 0 kg/m^3 when there are no new snow layers in the simulated snowpack.

The weak layer properties seem to follow the same trends at the two locations. The thickness decreases by some millimeters at Kroken, while it stays quite constant at Fjellet. The density increases over the whole period for both locations. The grain size and bond size increase at the beginning and then stabilize at both Kroken and Fjellet. These two properties vary slightly in scale, as the one at Fjellet has larger grain sizes and bond sizes overall.

Figure 13 depicts the two stability measures SK_{38} and SSI, as calculated by SNOWPACK, at both Kroken and Fjellet. The stability measure SK_{38} increases until the beginning of February, where it decreases until the end of February. After this, the measure stays quite constant, with some small fluctuations. The SSI follows the trend of the SK_{38} until the beginning of March for both locations. At this point, the SSI at Kroken increases by 1 for the rest of the simulation. The increase by 1 is a result of either a small hardness difference or grain size difference across the layer, as calculated by Equation 2.2.

5.4 Grouping the snowpack data into regimes

The new snow data and weak layer data are grouped into different regimes depending on the weather at a specific day t, as described in Chapter 3.1. Table 6 shows the different weather regimes. The effect of grouping the data into weather regimes impacts the model in different ways. Figure 14 shows a cross-plot for the new snow thickness in each regime at Fjellet, illustrating the relationship between the variable

at day t and day $t + 1$. The point size indicates the amount of precipitation at day $t + 1$. The point colors indicate the average temperature at day $t + 1$.

The grouping of regimes has an apparent effect on the new snow thickness at Fjellet. Some of the most apparent effects are

- LLH: The points above the straight line show the effect of wind on the new snow thickness. As there is a low amount of precipitation in this regime, the increase must result from high wind speed. Wind-drifted snow is a common cause of increased new snow thickness, especially when the wind speed is high.
- LHH: The points above the straight line show the effect of precipitation and wind on the new snow thickness. Precipitation and wind-drifted snow are common causes of increasing new snow thickness.
- HHH: The points below the straight line show the effect of warm temperatures on the new snow thickness. There is a high amount of wind and precipitation, which would typically increase the snow height. The snow thickness decreases in this regime, probably due to melting processes induced by the warm temperature.

Figure 15 shows the effect of grouping the data into different regimes on the new snow density at Kroken. The grouping of regimes has an apparent effect on the new snow density at Kroken. Some of the most apparent effects are

- LLH: The points above the straight line show that the combination of low temperatures, low amount of precipitation, and high wind speed increases the new snow density.
- HHH: The points above the straight line show that the combination of high temperatures, a high amount of precipitation, and high wind speed increases the new snow density.

Similar plots for the other variables are shown in Appendix A. Some regimes consist of fewer data entries, as the weather conditions of these regimes appeared less frequently over the simulation period. Careful analysis of this plot and the different crossplots in Figure 7.5 helped to determine threshold values for the regimes.

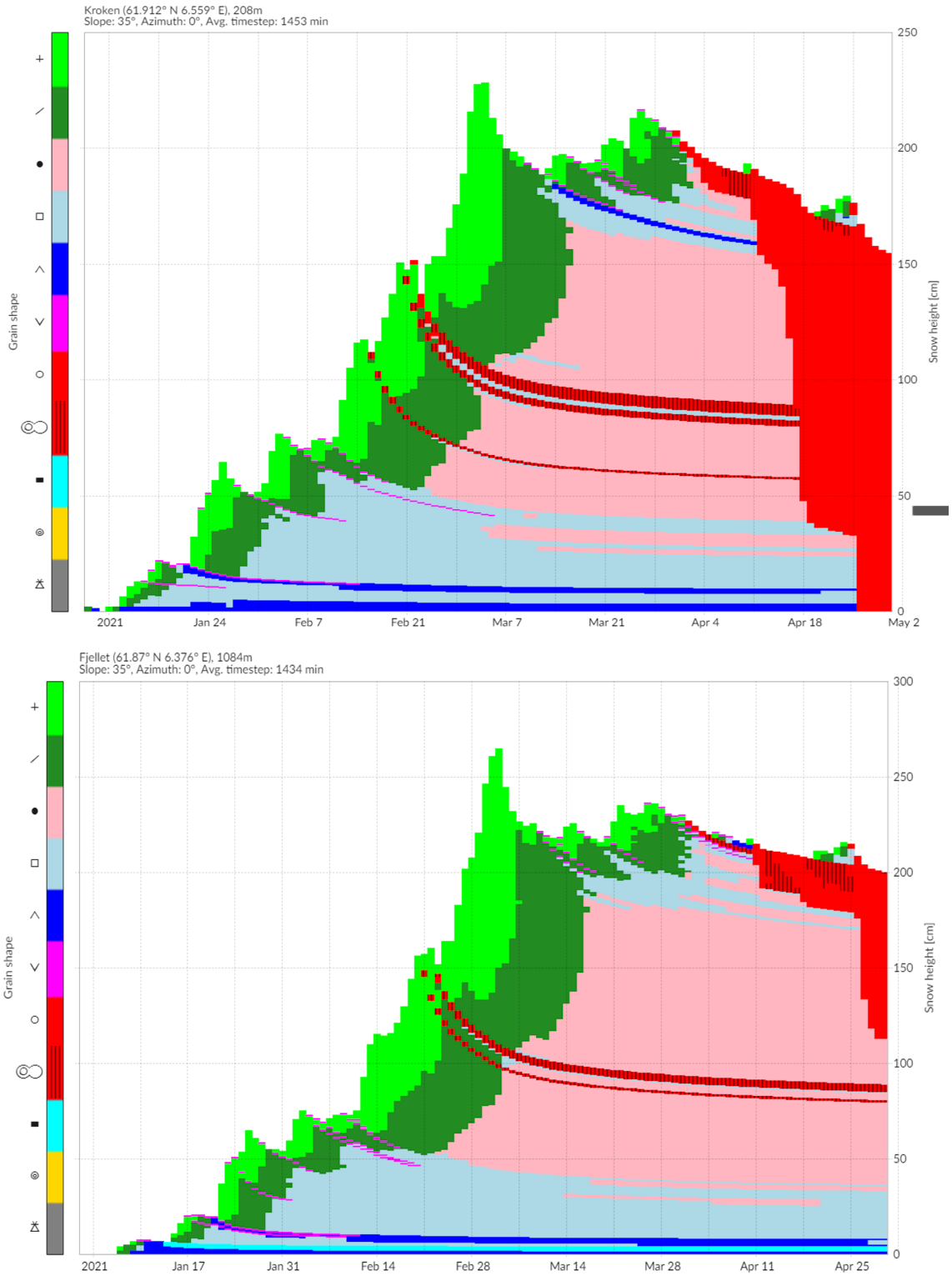

Figure 11: Simulation of snowpack at location Kroken a) and Fjellet b) respectively. The colors correspond to the grain types, see legend on left side of figure. The different snow grains are specified further in Chapter 2.1 and Table 1.

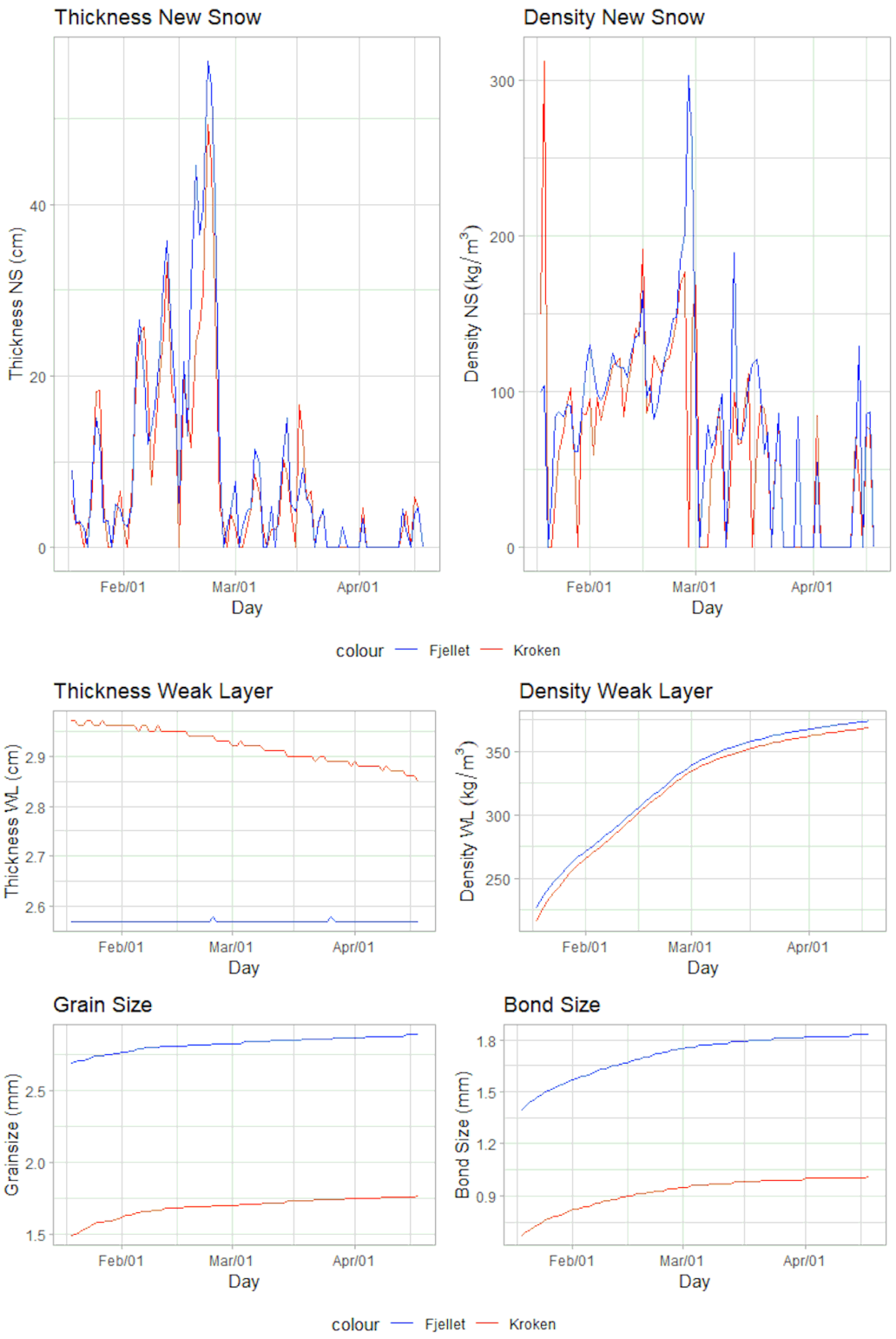

Figure 12: New snow layer properties and weak layer properties, as a time series, from January 18 to April 16. The red lines are for location Kroken, the blue lines for location Fjellet.

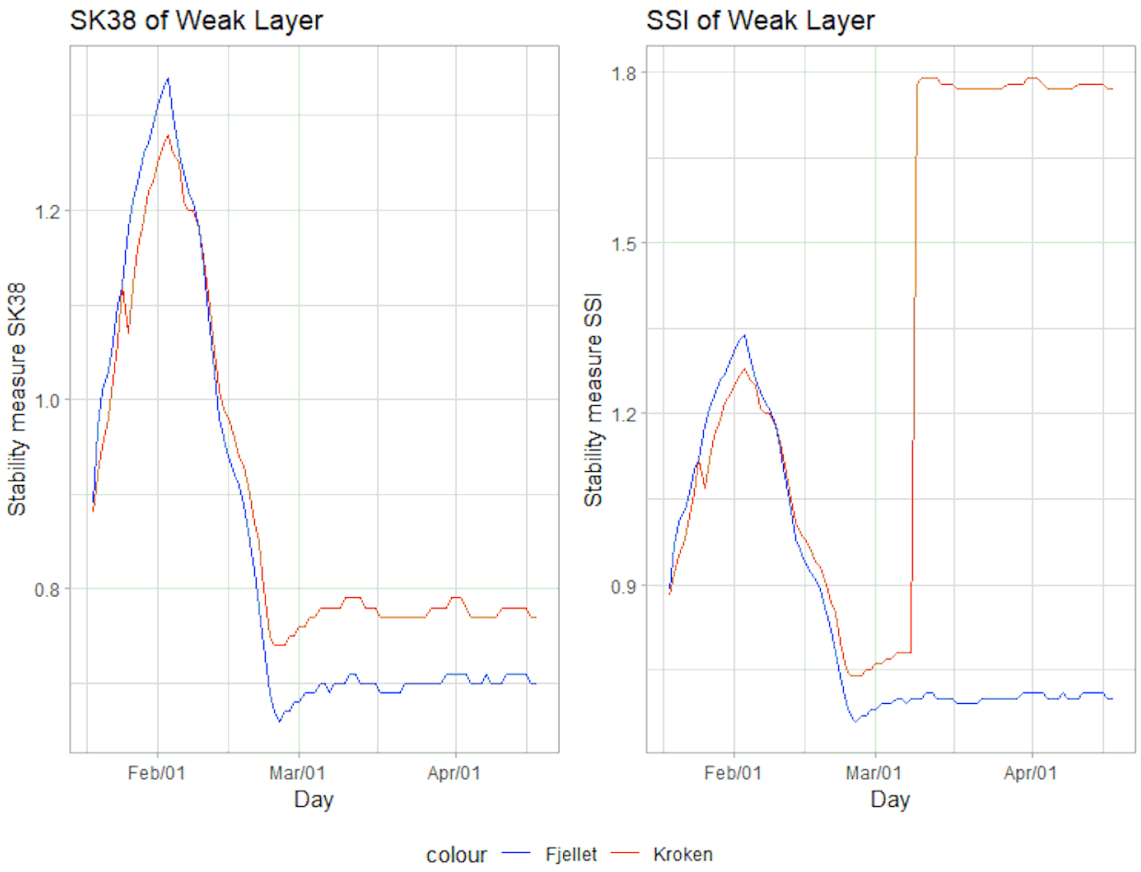

Figure 13: Timeseries of the simulated stability measures SK_{38} and SSI, from January 18 to April 16. The red lines are for location Kroken, the blue lines for location Fjellet.

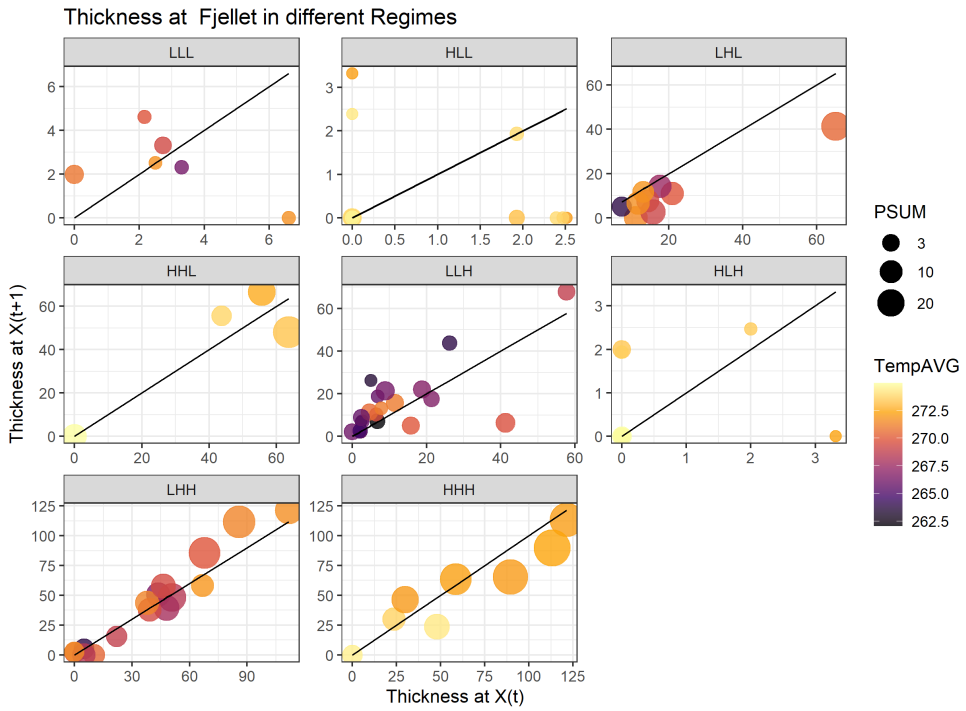

Figure 14: Cross-plot of new snow thickness in different regimes at Fjellet. The x-axis is the property value at t, the y-axis the property variable at $t + 1$.

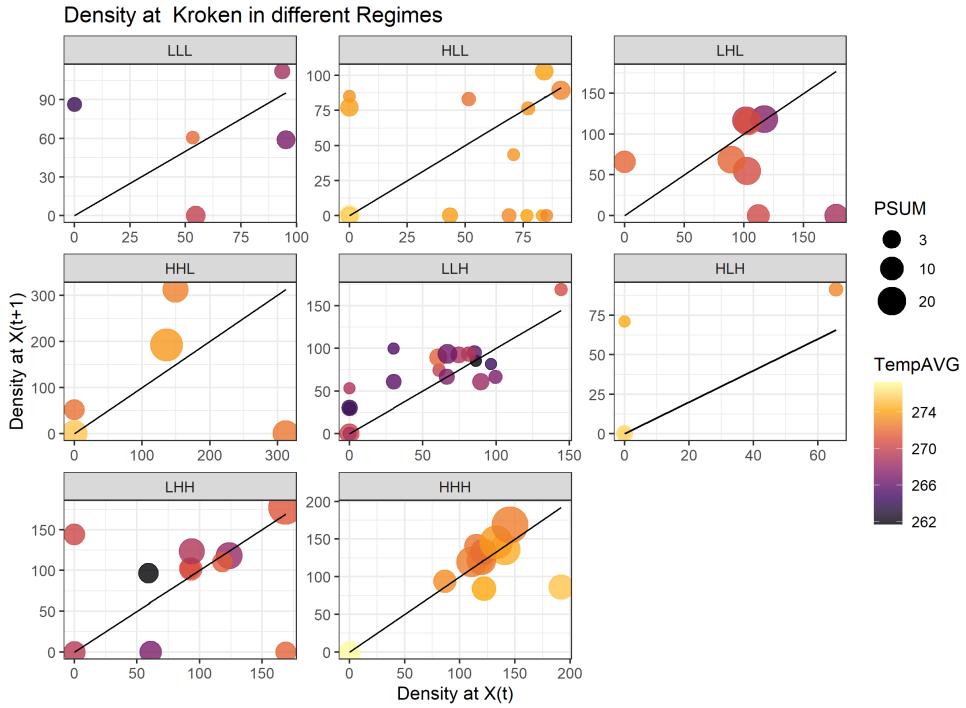

Figure 15: Cross-plot of new snow density in different regimes at Kroken. The x-axis is the property value at t, the y-axis the property variable at $t + 1$.

Chapter 6

Analysis and Results

This section presents the results of applying the Adaptive DLM to the data introduced in Chapter 5, focusing on Kroken. Chapter 6.1 presents the model and the determination of stability response variable, between SK_{38} and SSI. Two adaptive strategies are applied to the adaptive model. Let the adaptive model using the AMA strategy and the VOI strategy be denoted as the AMA-model and the VOI model, respectively. Chapter 6.2 analyses the results of a simulation with the AMA-model, compared to a non-adaptive model. Chapter 6.3 analyses the results of 100 simulations with the AMA-model, with both a fixed EST and an adjusted EST. Chapter 6.4 analyses the results of a simulation of the VOI-model, compared to a non-adaptive model.

The model uses simulated drone measurements, as the drone is not yet operational and ready to measure snowpack properties (as of May 2021). The proper data value at day t, with an assumed variance $\mathbf{\Sigma}_{t|0}$ linked to the drone, are used as drone measurements $\mathbf{d}_t$. See further discussion around this choice in Chapter 7. Initiation of a drone measurement is further denoted as a drone event in this thesis. The simulation period used in the results is from January 18 to April 16, 2021.

6.1 Model specifications

6.1.1 Initialising the model

Matrices $\mathbf{A}$ and $\mathbf{B}$ and the intercept $\boldsymbol{\gamma}$ are fitted on the data for each weather regime in R, using the method of ordinary least squares. Assume that the snowpack properties $\mathbf{X}_1$ is known at time $t = 1$, set to snowpack properties at Kroken at time $t = 1$.

$$\mathbf{X}_1 = (5.525,\ 149.06,\ 215.8,\ 2.97,\ 1.49,\ 0.67)^T \tag{6.1}$$

Assume the weather data $\boldsymbol{\omega}_{t+1}$ is known for every t. The available initial information is then as in Equation 3.10.

6.1.2 Determination of Stability metric

For each iteration, the DLM predicts r_{t+1}, the persistent weak layer's stability, as according to Equation 4.13. Both stability measures, SK_{38} and SSI, were fitted as a response variable using multivariate regression, with the snowpack variables as predictors. Both models had significant P-values, indicating correlations between the stability measures and the snowpack properties.

The SSI-metric determines the weak layer in the model and depends on discrete factors not included in the stability regression, such as hardness and grain size difference (see more in Chapter 2.3). As SK_{38} is simpler than SSI, it was determined more suitable as a response. The weak layer properties were the most significant variables for the model. Especially the thickness, grain size, and bond size showed high significance. Both new snow thickness and density showed the least amount of significance. The P-value showed that the model was overall highly significant. It also explained a large percentage of the variance; Adj$R^2 = 0.7086$.

6.2 One simulation using the AMA strategy

This section presents the analysis and results of using an adaptive DLM with an AMA strategy, as described in Chapter 4.3. See Algorithm 2 for details. The value of EST is set to 0.75. Chapter 7 discusses determining the EST-value. The probability threshold L is set to $L = 0.9$, so that the model initiates a drone event when $P(r_t \geq 0.75) \leq 0.9$. A simulation using a non-adaptive model is included to see the effect of the AMA strategy on the estimation.

Chapter 6.2.1 analyses the estimated properties of the simulation, and Chapter 6.2.2 analyses the predicted stability. Chapter 6.2.3 analyses the uncertainty of the stability predictions. It is important to clarify that this is one possible realization of the property estimation, based on ultimately a low amount of data. Another simulation of the model could therefore produce somewhat different results. This is further discussed in Chapter 7.

6.2.1 Properties

Figure 16 shows the new snow properties, and Figure 17 shows the weak layer snow properties for both the adaptive and non-adaptive models. The blue line is the modeled properties using the AMA-model, while the orange line is the modeled properties of the non-adaptive model. The yellow points indicate the days of a drone event.

The model initiates the first drone event on February 25. After the drone event, the model updates the snow properties using the newly obtained drone measurement, which significantly impacts the modeled snow property distributions. Figure 16 shows the effect of the updated model distribution on the new snow thickness and density.

The new snow thickness, in particular, shows apparent differences between the AMA-model and the non-adaptive model. After a drone measurement, there is a decrease in new snow thickness for the AMA-model, while for the non-adaptive model, it increases a significant amount. At a particular time, the non-adaptive model estimates the new snow thickness to be over 2 m high, while it decreases to close to 0 m for the AMA-model.

A reason for the high increase in estimated new snow thickness by the non-adaptive model directly after the first drone event could be the weather conditions. The weather conditions in this period consist of a high amount of precipitation, high wind speed, and warm temperatures, which normally lead to an increase in new snow thickness. The non-adaptive model may exaggerate weather effects when estimating new snow thickness. The AMA model's decrease in estimated new snow thickness shows the strength of updating the model with more accurate drone measurements.

Another reason for the difference in estimated new snow thickness after a drone event is the uncertainty of the models. The estimation by the non-adaptive model fluctuates a large amount compared to the AMA-model in March. This suggests that the variance is substantially higher for the non-adaptive model in this period compared to the AMA-model, making the estimations less reliable. In April, the new snow thickness of both the non-adaptive and the AMA-model drops to zero. This is probably due to April being a spring month, where the most prominent weather regimes have high temperatures. It could also be because the weather in April was quite dry (see Figure 10).

Uncertainty propagation could explain the differences in the new snow thickness between the two models. The estimated variance $\hat{\mathbf{\Sigma}}_{t+1|t}$ at time $t+1$ depends on the variance $\hat{\mathbf{\Sigma}}_{t|t}$ at time t. Thus as the model develops with time, the uncertainty propagates, leading to less accurate predictions. After a drone event, however, the variance seems to decrease, resulting in less fluctuation. The decrease is due to the drone measurements having less uncertainty compared to the estimated properties. Chapter 6.2.3 further analyses the predicted stability uncertainty.

Another explanation for the high variance in the non-adaptive model in March is the weather regimes prominent in this period. The data was fitted on the grouped data, corresponding to the 8 different weather regimes. Some of the regimes consisted of fewer data entries, leading to a higher variance in these regimes (see Table 6 for the different weather regimes). The period between the end of February and the beginning of March had a high amount of precipitation and moderately high temperatures (see Figure 10). This regime was less common in the dataset, resulting in more variance.

There are fewer differences in the new snow densities, as estimated by the two models. Compared to the AMA-model, the non-adaptive model estimates higher densities at the beginning of March and lower densities at the end of March. The

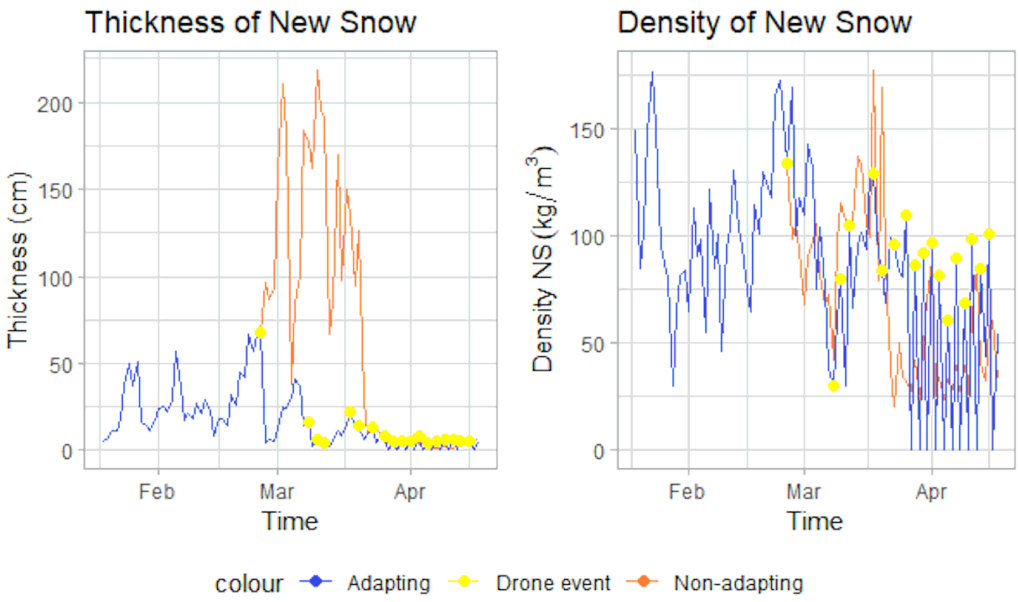

Figure 16: Time series of the new snow layer properties for both the adaptive and non-adaptive models, from January 18 to April 16. The blue line is the AMA-model, the orange line is the non-adaptive model, yellow points are drone events.

AMA-model remains relatively consistent throughout the simulation. An apparent problem with the AMA-model is noticeable in April. A drone monitored the snow thickness to zero, leading necessarily to the density decreasing to zero. As there are many drone events in this period, there are also many zero-values in the estimated densities.

Figure 17 shows the modeled weak layer properties by the adaptive and non-adaptive models. The weak layer thickness decreases over time, while the grain size, bond size, and snow density increase over time. The faceting processes discussed in Chapter 2.1 explain the development of weak layer properties and indicates that the weak layer plotted is a persistent weak layer buried in the snowpack. The weak layer properties show less fluctuation than the new snow properties, indicating less variance.

Some important results of updating the model with drone measurements are apparent when comparing to the non-adaptive model. After the first drone event, the AMA-model estimates a larger weak layer thickness, grain size, and bond size than the non-adaptive model. The adapting model consecutively estimates the thickness higher than the non-adaptive model. There is also less fluctuation in the estimated thickness of the AMA-model compared to the non-adaptive model. Bond size and grain size curves flatten earlier for the AMA-model than for the non-adaptive model. The smaller fluctuation and earlier flattening are possibly due to frequent drone events, decreasing the model uncertainty. The density plot shows fewer differences between the two models.

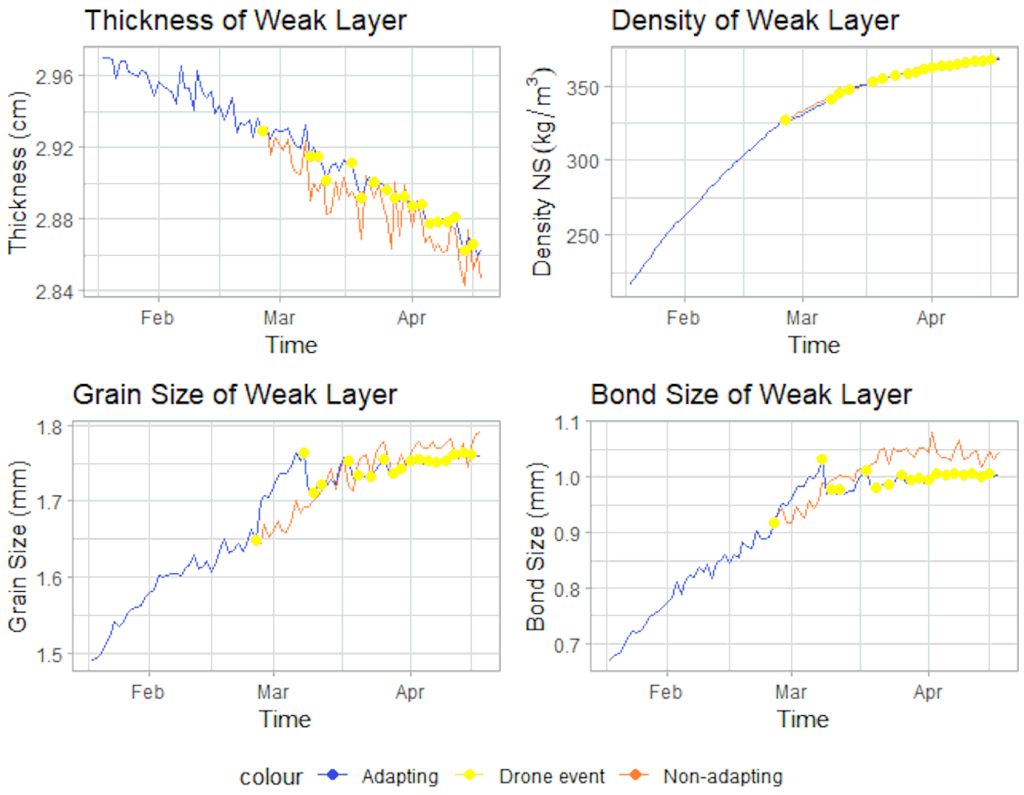

Figure 17: Time series of the the weak layer properties for both the adaptive and non-adaptive models, from January 18 to April 16. The blue line is the AMA-model, the orange line is the non-adaptive model, yellow points are drone events.

6.2.2 Stability

Figure 18 shows the predicted stability for every day in the simulation for both the adaptive and the non-adaptive model. The dotted red line indicates the EST, set to EST = 0.75. The predicted stability is every day put to a threshold-test, testing whether $P(r_t > \text{EST}) < 0.9$ (see Chapter 4.1). The arrow in the plot points to the first drone event initiated by the model.

There is a noticeable difference in the predicted weak layer stability, as predicted by the adaptive and the non-adaptive model after the first drone event. The AMA-model predicts that the weak layer stability increases, while the non-adaptive model predicts that the weak layer stability decreases. The predicted stability stays above the threshold for multiple weeks for the AMA-model, while for the non-adaptive model, the stability fluctuates and quickly drops beneath the threshold line. After the second drone event in March and beyond, the non-adaptive model predicts weak layer stability below EST, indicating that the layer is potentially unstable. The AMA-model, meanwhile, predicts stability above the threshold, indicating that it is stable. It is apparent that the non-adaptive model is somewhat pessimistic and

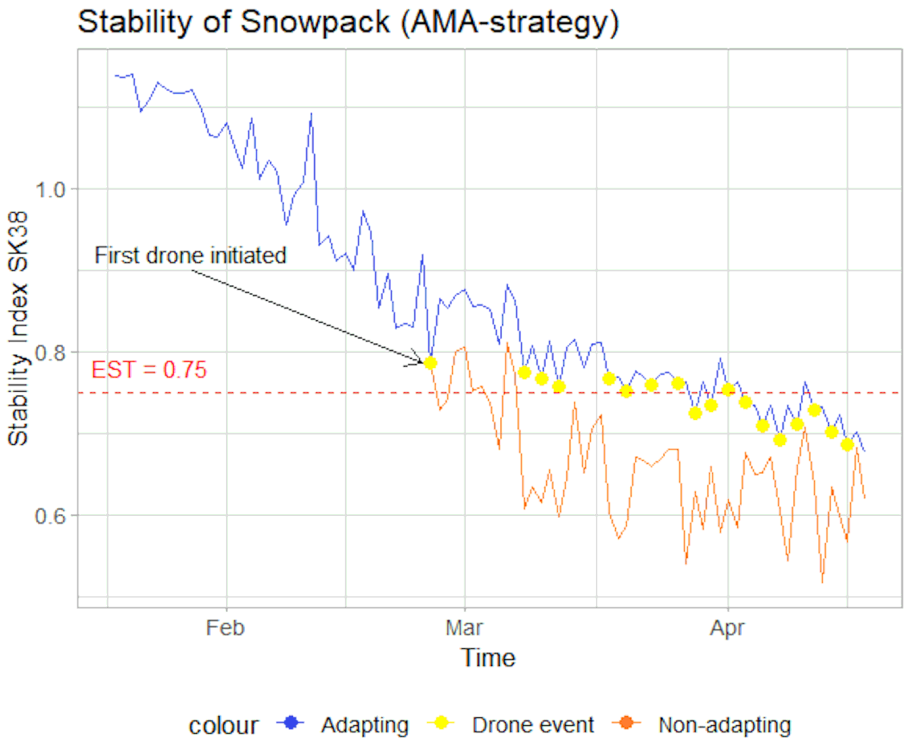

Figure 18: The predicted stability of the weak layer of the snowpack for each day t, from January 18 to April 16. The yellow points are the drone events. The blue line is the AMA-model, the orange line is the non-adaptive model.

generally predicts lower stability compared to the AMA-model.

The AMA-model predicts stability above the threshold in most of March, while the non-adaptive model predicts stability below the threshold in the same period. March is, however, a period of frequent drone events, indicating that the model predicts that there is less than 90 % probability that the stability is higher than the EST. Notice that the stability predicted by the non-adaptive model fluctuates much more than the stability predicted by the AMA-model. There is more variance when simulating with the non-adaptive model than with the AMA-model. One reason is the high number of drone events, resetting the variance propagation. Another reason is the large fluctuations in the new snow properties in March, as described in Chapter 6.2.1.

6.2.3 Uncertainty

Figure 19 shows the predicted stability using the AMA-model, alongside a prediction interval with a confidence band of one standard deviation. The variance seems to increase as the model develops with time, resulting in more uncertain predictions. Notice immediately after the first drone event, at the end of February, the uncertainty

decreases. After receiving more accurate measurements from the drone, the uncertainty propagation resets, leading to more accurate stability predictions and decreased variance.

Figure 20 shows a similar plot for the non-adaptive model. Notice that the uncertainty seems to increase over the whole simulation period. The increasing uncertainty results in less accurate predictions as time develops. The difference in uncertainty between the two models shows the AMA-model's strength: the AMA-model yields more accurate stability predictions by resetting the uncertainty propagation after a drone event.

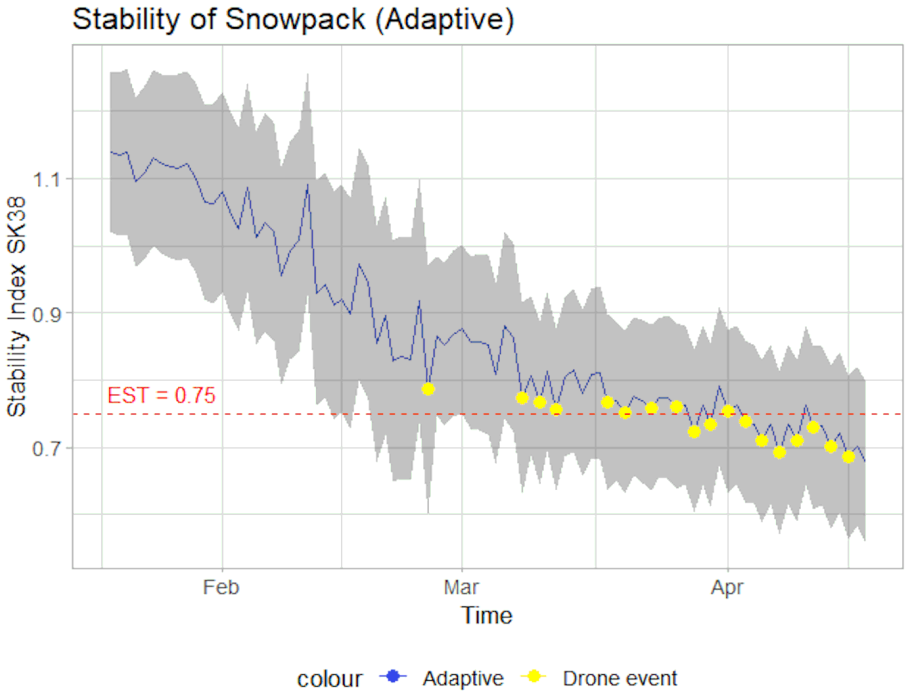

Figure 19: Predicted stability of weak layer with confidential band of 1 standard deviation, for the period January 18 to April 16, using the AMA-model.

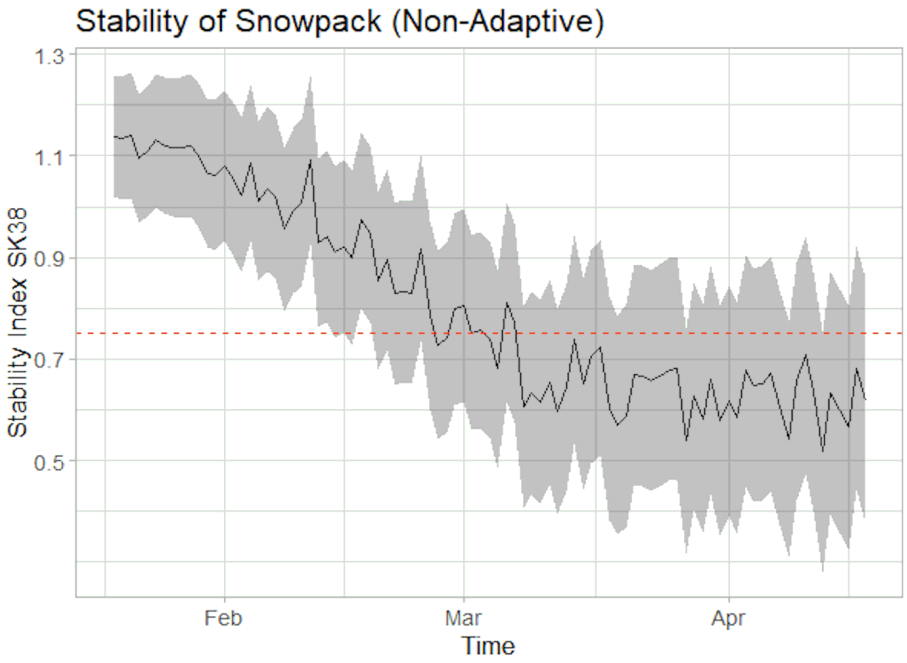

Figure 20: Predicted stability of weak layer with confidential band of 1 standard deviation, for the period January 18 to April 16, using the non-adaptive model.

6.3 100 simulations using the AMA strategy

This section shows some general results of the AMA-model, after running 100 simulations. The focus is the predicted weak layer stability, the number of drone events, and how many days until the first drone event. In Chapter 6.3.1 the threshold EST is fixed, to EST = 0.75. Chapter 6.3.2 explores the model performance when adjusting the threshold EST.

6.3.1 Fixed parameters

Figure 21 shows two bar plots. The bar plot on the left shows the number of first drone events on a particular day over the 100 simulations. The range of the first drone event is between day 32 and 44 (February 19 to March 3), while a majority occur between day 35 and 38 (February 22 to February 25). Day 38 (February 25) has the highest counts of first drone events overall. The bar plot on the right shows the number of drone events over the 100 simulations. All the simulations initiate between 14 and 20 drone events, and a majority of the simulations initiate 17 or 18 drone events.

Figure 22 shows the predicted stability of 100 simulations of the AMA-model. The blue line is a smoothed trend line, indicating the general trend of the simulations. Notice the similarities between the predicted stability using 100 simulations and the predicted stability of the single simulation described in Chapter 6.2. The predicted stability decreases until late February, where the curve flattens. Late February is

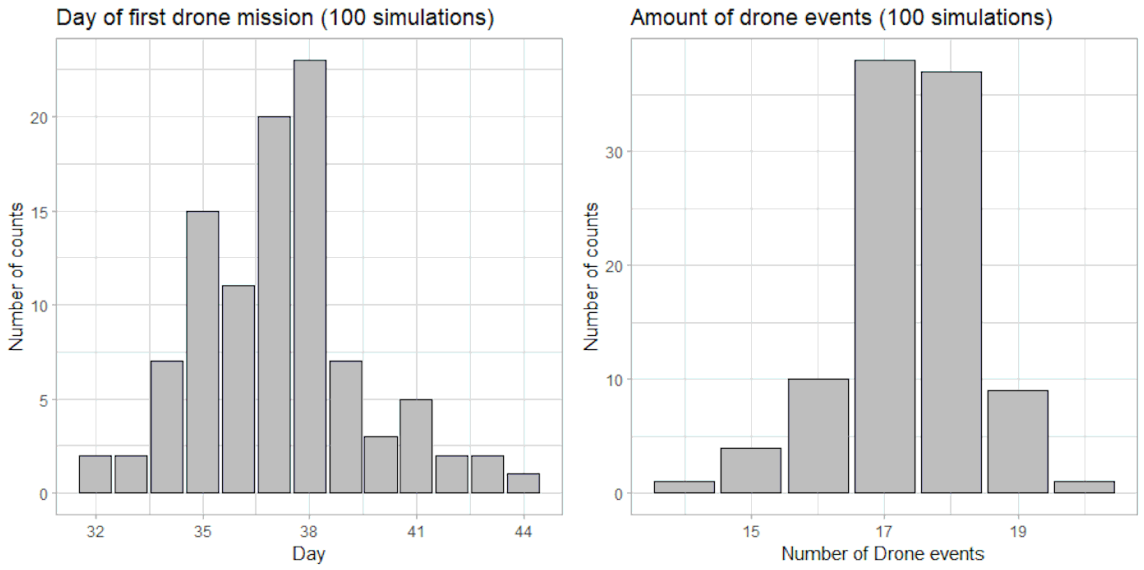

Figure 21: Count data of day of first drone event (left) and number of drone events (right) over a 100 simulations.

when most first drone events occur, showing the impact of a drone event. In March, the predicted stability starts to decrease before it again flattens in the middle of March. From April and onwards, the stability decreases slowly. The predicted stability decreases when not updated with drone measurements and stays flat when updating with drone measurements. This shows that the non-adaptive model is quite pessimistic compared to the AMA-model.

The curve fluctuates close to the EST between the middle of March and the beginning of April. This is a period of frequent drone events, routinely updating the model with more accurate measurements. The fluctuation is highest from the middle of February to the middle of March, and the lowest from the middle of March to the end. As time develops, the fluctuations increase, a result of uncertainty propagation. In the last period of March and beyond, the fluctuations are much smaller, most likely because of frequent drone events, updating the model distribution with less uncertain data.

6.3.2 Adjusting parameters

The determination of a suitable threshold-value EST plays an important part in the AMA-model (see Algorithm 2). In the simulations described previously, the stability threshold was fixed to EST = 0.75, as multiple sources reported a stability measure of 0.75 or lower as potentially unstable. The choice EST = 0.75 is derived from a combination of reports and therefore noted as an expert choice. However, some conflicting reports indicate different thresholds for a potentially weak layer (see

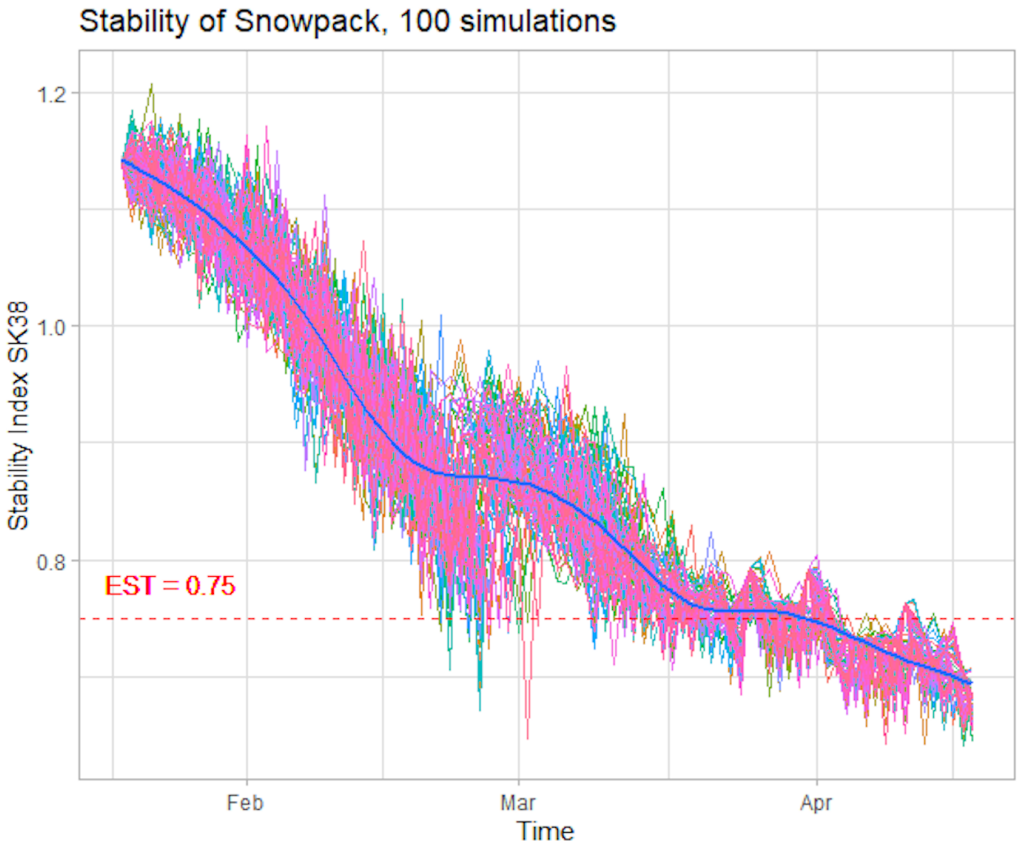

Figure 22: Predicted stability of weak layer over a hundred simulations, for the period January 18 to April 16, using the AMA-model.

Chapter 2.3). Chapter 7 discusses the determination of EST further. This section investigates how the AMA-model performs with different EST-values in regards to the number of drone events and how long time before the first drone event.

Figure 23 shows the average day of the first drone event and the number of drone events for different EST-values after running 100 simulations for each value. EST-values used in the simulations are in the range $[0.6, 1.1]$. The figure on the left shows that lower EST-values delay the initiation of drone events. As the EST-value increases, the days before the first drone event decreases linearly. The figure on the right shows that lower EST-values result in fewer drone events and that the number increases when EST increases. The steepest increase of drone events happens when EST increases from 0.65 to 0.80. In this period, the number of drone events increases from 4 events to 22 events. The maximum number of drone events happen when the EST = 1.1, with over 40 initiated events.

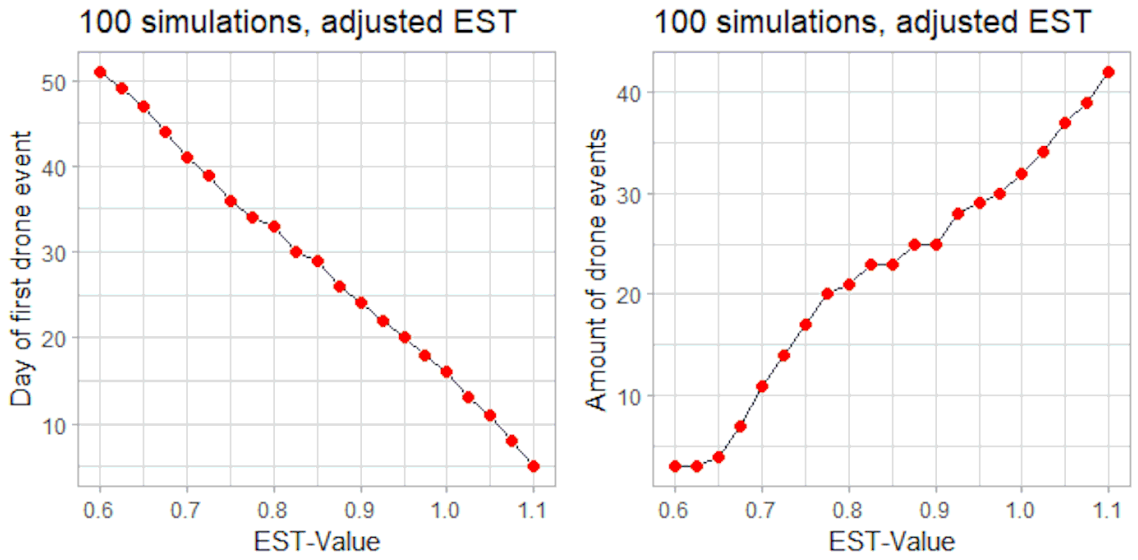

Figure 23: Predicted stability of weak layer over a hundred simulations, for the period January 18 to April 16, using the AMA-model with different EST-values.

6.4 VOI approach

This section presents the results of using a Value of Information strategy to model the stability (see Algorithm 3). This model requires the determination of certain parameters, including L_{VOI}, EST, and the costs C_0 and C_1. Figure 6.4 shows a simulation of the VOI-model with fixed parameters EST $= 0.75$, $L_{\text{VOI}} = 0.5$, $C_0 = 1$ and $C_1 = 100$. The cost parameters indicate that the cost associated with keeping a road open when unstable is 100 times larger than closing the road. This approach is important regarding snow avalanche probability, as there is a high cost associated with a road blocked by an avalanche. The figure on the left is the snowpack stability over the whole period, with a confidential band of one standard deviation. Here, the yellow points are the days of drone events during the simulation.

The figure on the right is a plot of expected VOI over time. When the VOI is higher than L_{VOI}, the VOI-model initiates a drone event. The first drone event occurs at the end of February. After the event, the stability increases directly, as for the AMA-model. As the VOI drops down to 0 after the first drone event, there is not much value in initiating new drone events at this time. From the middle of March and further, the VOI stays high, initiating frequent drone events. As there are more drone events in the latter part of the simulation, it is apparent that the value of a drone measurement is high at this point. The VOI-model initiates 20 drone events with the fixed parameters, similar to the number of drones initiated with the AMA strategy, as described in Chapter 6.3.1.

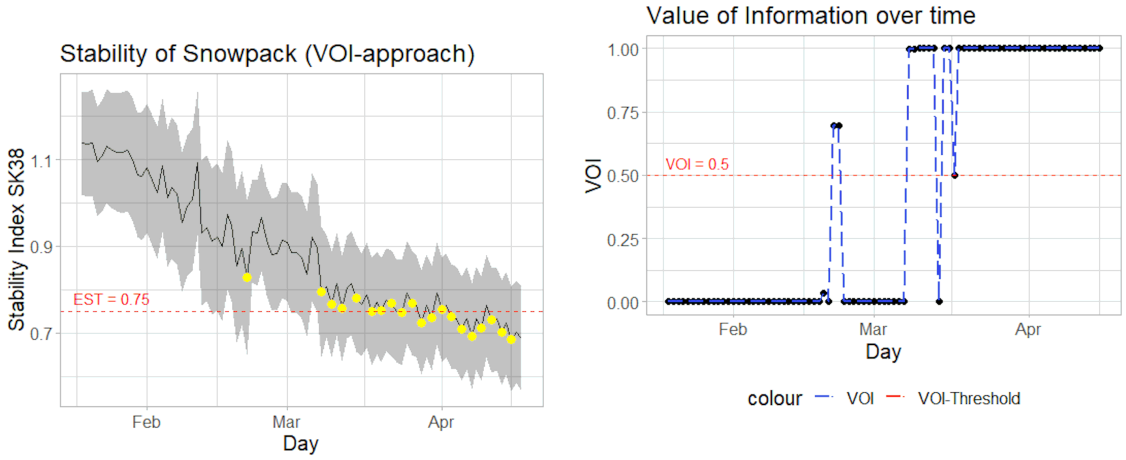

Figure 24: Predicted stability and expected Value of Information over time, using the VOI-model.

Figure 25 illustrates the effect that the cost-parameters has on the VOI-model, where C_0 is fixed to 1. When the cost C_1 is low, the VOI-model delays initiating the first drone event. Notice that for low C_1-values, when $C_1 = 4$ and $C_1 = 5$, the first drone event is initiated after the predicted stability is less than the threshold-line. When the cost C_1 increases, there is more value in a drone measurement. Notice that when $C_1 = 10$ and $C_1 = 100$, the first drone event happens when the predicted stability is far from the threshold line. There is an intuitive reason for the effect of cost on the initiation of drone events. When there is a low cost associated with keeping the road open, even though the predicted stability is low, there is less value of information in the drone measurement. The VOI-model then waits until critical conditions regarding the predicted stability to initiate the drone. When the cost C_1 is high, there is more value of information associated with a drone measurement, resulting in earlier drone events and a higher number of drone events.

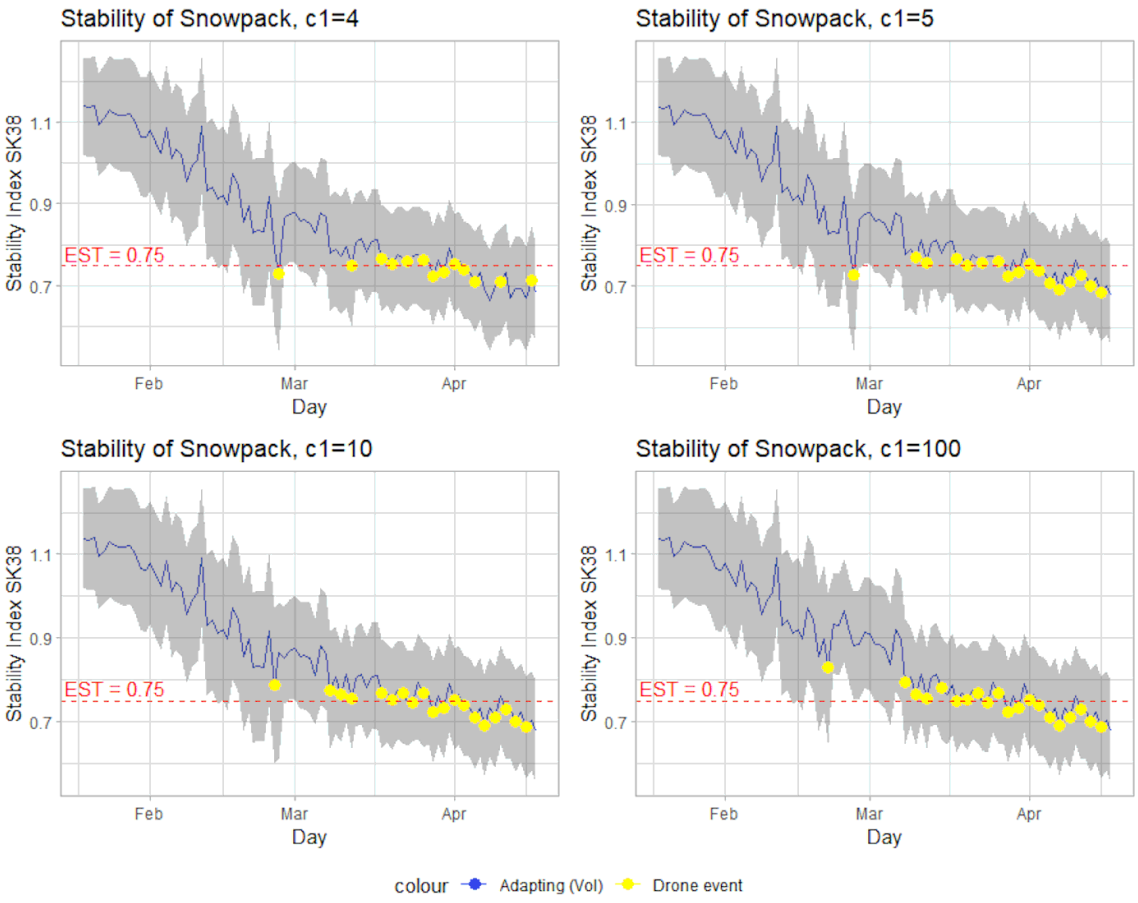

Figure 25: Predicted stability using the VOI-model with different C_1 parameters.

Chapter 7

Discussion and Conclusion

This thesis has developed a data-driven statistical model that predicts the stability of a weak layer in a snowpack based on estimated weak layer properties and new snow properties. SSI is a stability measure used to determine the weakest layer in the snowpack. The model predicts the stability by a multivariate regression model, with the estimated snow properties as predictors and the stability measure SK_{38} as a response.

This chapter discusses some of the main points of this thesis. Chapter 7.1 discusses the use of uncommon data sources such as SNOWPACK, WxGen, and drone measurements when predicting stability. The determination of EST used in the results of this thesis is discussed in Chapter 7.2. The key results of the model are presented in Chapter 7.3. Some limitations of the model are discussed in Chapter 7.4, and some further works of the model are discussed in Chapter 7.5.

7.1 Additional Data Sources

An important motivation for this thesis is incorporating data not typically used in Norway's monitoring systems. This includes weather data generated from WxGen, numerical snowpack properties simulated by SNOWPACK, and the properties measured using a drone from the GeoDrone-project. WxGen is primarily used to get the weather data required by SNOWPACK, including incoming solar radiation, a measurement not typically monitored at the weather stations in Norway. WxGen allows the user to generate numerous independent weather scenarios, each within historical trends, for arbitrarily selected locations. Therefore, it should be easy to change the study area and add more data to the model if necessary. Varsom, the primary warning/monitoring system in Norway, relies on weather data and manual stability tests. Using numerical models and drone measurements provides information otherwise unavailable, such as the snowpack properties and quantitative stability measures for each layer, increasing the data available to the forecaster.

Simulating the snow cover with SNOWPACK and extracting the chosen properties was more time-consuming than anticipated, requiring a great effort by the user. Hopefully, some of the work done in this thesis can help others using similar methods. First, the user must preprocess the weather data into a file format permitted by SNOWPACK. Most weather data is in a NetCDF format, including the weather data from WxGen or JSON (Javascript Object notation). SNOWPACK has some plugins available for NetCDF, but the program requires a good knowledge of C++ to compile the plugins. The recommended file format is called SMET, a format developed by the SNOWPACK authors. SNOWPACK produces hourly measurements of numerous properties for each layer in a snowpack over the whole simulation period, resulting in a large dataset. Post-processing is required to get the chosen properties for the specific snowpack layers at $12:00$ every day, including finding the weak layer in the snowpack and extracting its properties. Appendix B includes the code in R used to extract the NetCDF file from WxGen and convert it to the SMET format, and also the code used in extracting the relevant properties from the output of SNOWPACK.

7.2 Estimated Stability Threshold

The model incorporates two strategies to initiate and update the model with drone measurements, denoted as an AMA-model and a VOI-model. The AMA-model initiates drone events when there is less than 90 % probability that the predicted stability is higher than the EST. The VOI-model initiates drones when the expected value of information in a drone measurement is higher than a threshold. A model utilizing a non-adapting strategy without any external drone measurements is included in the results to compare the models.

Both the AMA-model and the VOI-model depend on the determination of EST. EST is a threshold that indicates that a layer is potentially unstable. In this thesis, EST is mainly fixed to $EST = 0.75$. This fixed value was a result of studying different reports using similar thresholds for potential instability. There are some limitations of the SSI and SK_{38} measures, as there is no physical sense that the weak layer stability has a decreasing trend over the whole winter period. The stability should rather have some cycles of increase and decrease over the winter. There are probably some limitations to the physical model of SK_{38} and SSI. It is therefore not reasonable to predict that a weak layer will collapse solely based on the stability metric SK_{38}. Still, the predicted stability and its development over time indicate the instability of a weak layer. To get additional information about the snowpack stability, one could use the drones to investigate the snowpack surface with the drone cameras for potential signs of avalanche formation and fractures, in addition to monitoring the properties.

7.3 Key results

The results compared the model performance of both the AMA-model and the VOI-model with a non-adaptive model.

7.3.1 Properties

The results include an extensive comparison between estimated snow properties by the AMA-model and the non-adaptive model. New snow thickness and density showed large differences, most noticeably directly after the first drone event. A reason for the differences could be that the non-adaptive model exaggerates the effect of weather on the snow properties. This was most apparent after the first drone event in March, where the non-adaptive model estimated a high increase of new snow thickness while the adaptive model decreased. The estimated new snow properties of the non-adaptive model also fluctuated more prominently than for the AMA-model. There were also some differences in the weak layer properties estimated by the two models. The properties estimated by the AMA-model generally fluctuated less than the properties estimated by the non-adaptive model.

7.3.2 Stability

The predicted stability was higher for both the AMA-model and the VOI-model compared to the non-adaptive model. It seems that the non-adaptive model exaggerates the instability of a weak layer in general. This exaggeration was most apparent right after the first drone event, where the predicted stability increased for the adaptive model and decreased for the non-adaptive model. A possible explanation for the difference is that the non-adaptive model has a continuous uncertainty propagation over time, resulting in more uncertain stability predictions as time develops. By updating the model distribution with more accurate drone measurements, the adaptive models predicts weak layer stability with less uncertainty.

7.3.3 Parameters

The number of drone events and the number of days before the first drone event for the AMA-model depends on the EST-value. Low EST-values resulted in few drone events and a long time before the first drone event. Meanwhile, high EST-values resulted in a high number of drone events and a low number of days before the first drone event. For the VOI-model, the cost parameters C_0 and C_1, in particular, affected the number of drone events and the number of days before the first drone event. When the cost C_1 of keeping a road open when predicted stability is less than EST was similar to the cost of closing a road, the expected value of information in a drone measurement was smaller, resulting in a late first drone event and few drone events overall. When the cost parameter C_1 was much larger than C_0, however, there was a higher number of drone events and an earlier date for the first drone event.

7.4 Model limitations

The dataset used to generate the dynamic model is based on snowpack properties and weather data mainly linked with a single study area in Stryn, not analyzing different areas in Norway. The data is obtained from two locations in Stryn, Kroken, and Fjellet, over a single winter period, consisting of 89 days. The results show only one realization of estimated snow properties and predicted stability. The weather regimes and the strategies developed could work differently for other weather, snow, and risk simulations, which need to be explored for further use. A natural extension of this model is to incorporate spatial features, such as spatial correlations and clustering between different locations to make the model regional. The same strategy used in this thesis should be applicable elsewhere, as the data generators SNOWPACK and WxGen can be used in arbitrary locations.

A limitation of the model is the small amount of data, leading to high variances in some weather regimes. A larger dataset, consisting of multiple locations in the area, and an extension of the simulation periods, could decrease the model uncertainty, resulting in more accurate predictions. It is not much extra work to simulate multiple snowpacks using SNOWPACK, given that the weather scenarios generated by WxGen are independent and stays within historical trends.

The drone measurements had to be simulated, as the real-time processing part of the GeoDrone project is still in the developing stage (spring 2021). The accuracy and uncertainty associated with the drone measurements had to be chosen based on the drone resolution. A drone equipped with GPR should have a small uncertainty when measuring some properties, such as thickness and density. Measurements of grain size and bond size would probably have more associated uncertainty, as they would need to be calculated by some correlation methods. Nevertheless, drone measurements should be more accurate than the estimated snow properties, so updating the model using simulated drone measurements is comparable with actual drone measurements. This aspect needs to be inspected more carefully when the real-time processing part of the GeoDrone project is available.

Snow avalanche formation is a highly complex process involving weather effects, metamorphism effects within the snowpack, and a weak layer's development over time. The Adaptive Dynamic Linear Model used to develop the snowpack properties over time is simplified, only including some of the factors and properties linked with the stability of a weak layer. It is not wholly reasonable to believe that the predicted mechanical stability measure can predict critical stability and avalanches. More extensive models need to be implemented, adding more features and more sophisticated data-driven methods, such as a neural network and random forest over more extensive data sets. The simple model was chosen due to the short time frame of the master thesis and a large amount of time used to generate the data. It was also chosen because it easily could incorporate the updating part of the model and supported

using different strategies to initiate the drones. A more data-extensive model would need a different approach regarding updating with drone measurements.

The adaptive model developed in this thesis can indicate the potential instability of a weak layer. It should be possible to combine this model with other forecasting models used in Norway. The data uses numerical snowpack data, drone data, and weather data, making it an interesting addition to the warning system in Norway, as they mainly rely on weather data and manual stability tests.

7.5 Further works

A natural extension of the model is to add spatial effects, making the model applicable regionally in Norway. Adding spatial correlations and clustering effects for different parts of Norway should be possible, as the data used in the model can be generated at arbitrary locations. WxGen generates data in a gridded spatial data format if requested by the user, which could be used as input to simulate snow covers with SNOWPACK in different locations in Norway. Another interesting spatial extension could be to model different locations in a snowpack and add spatial correlations between the different locations, especially as drone measurements allow more information about the spatial variability of the snowpack. For example, if a large snowpack is situated on a slope with a road beneath. The model could then predict the stability at different locations in the snowpack and choose the most critical part to monitor. SNOWPACK allows gridded data as input and makes it possible to simulate 2D-gridded snowpacks, which can be helpful in this regard.

Another extension is further developing the strategies initiating drone events. The VOI strategy is especially interesting, as it can have a substantial financial impact, helping those responsible for closing roads and monitoring road safety. In this thesis, the decision rule depends on the possible cost of predicted low stability when not closing the road, compared to the cost of closing the road. Other possible alternatives could be added to the strategy so that different VOI thresholds initiate different methods to monitor the snowpack or trigger the avalanche artificially (using explosives). Examples of strategies that could add to the VOI strategy are listed in Table 7. These strategies would each have an associated cost, resulting in a practical and financial application of the model.

Alternative 1:	Drone - GPR
Alternative 2:	Drone - GPR, LIDAR
Alternative 3:	Drone - GPR, LIDAR, Manual stability tests
Alternative 4:	Launch the avalanche with explosions
Alternative 5:	Close road
Alternative 6:	Do nothing - Let Avalanche Fall (blocking road)

Table 7: Possible scenarios that can be incorporated into a VOI strategy for further works.

Bibliography

American Avalance Center, & National Avalanche Center. (n.d.-a). *The physical change of snow grains due to differences in temperature and pressure.* Retrieved February 7, 2021, from https://avalanche.org/avalanche-encyclopedia/metamorphism-snow/

American Avalance Center, & National Avalanche Center. (n.d.-b). *Stability.* Retrieved April 26, 2021, from https://avalanche.org/avalanche-encyclopedia/stability/

Avalanche Canada. (n.d.). *Glossary.* Retrieved May 27, 2021, from https://www.avalanche.ca/glossary

Bavay, M., & Egger, T. (2014). Meteoio 2.4.2: A preprocessing library for meteorological data. *Geoscientific Model Development*, *7*(6), 3135–3151.

Bellaire, S., Schweizer, J., Fierz, C., Lehning, M., & Pielmeier, C. (2006). Predicting snow cover stability with the snow cover model SNOWPACK, 38–43.

Dupuy, B., Tobiesen, A., Grøver, A., Einbu, A., & Romdhane, A. (2021). Drone geophysics for forecasting and monitoring natural hazards. [in press]. *EAGE Near Surface Geoscience*.

Eidsvik, J., Mukerji, T., & Bhattacharjya, D. (2015). *Value of Information in the Earth Sciences: Integrating Spatial Modeling and Decision Analysis.* Cambridge University Press. https://doi.org/10.1017/CBO9781139628785

Jamieson, J. B., & Johnston, C. (1998). Refinements to the stability index for skier-triggered dry-slab avalanches. *Annals of Glaciology*, *26*, 296–302.

Mayer, S., Herwijnen, A., & Schweizer, J. (2021). A random forest model to assess snow instability from simulated snow stratigraphy. *EGU General Assembly 2021.* https://doi.org/https://doi.org/10.5194/egusphere-egu21-12259

Monti, F., & Schweizer, J. (2013). A relative difference approach to detect potential weak layers within a snow profile.

Monti, F., Schweizer, J., & Gaume, J. (2014). Deriving snow stability information from simulated snow cover stratigraphy.

Müller, K. (2019a). *Snø og snøskred.* [PowerPoint-presentation]. Retrieved February 7, 2021, from https://www.varsom.no/snoskredskolen/kursmateriell-og-film/?ref=mainmenu

Müller, K. (2019b). *Snøomvandling mellom hovedklassene.* [PowerPoint-presentation]. Retrieved February 15, 2021, from https://www.varsom.no/snoskredskolen/kursmateriell-og-film/?ref=mainmenu

National Snow and Ice Data Center. (n.d.). *All about snow: How snow forms.* Retrieved February 5, 2021, from https://nsidc.org/cryosphere/snow/science/formation.html

Norges Geotekniske Institutt. (n.d.). *Avalanches.* Retrieved April 27, 2021, from https://www.ngi.no/eng/Services/Technical-expertise/Avalanches

Norges Vassdrag- og Energidirektorat. (n.d.). *xGeo.* Retrieved May 27, 2021, from http://www.xgeo.no/index.html?p=fag

Norges Vassdrag- og Energidirektorat. (2016). Fakta: Snøskred - tørre og våte. Retrieved February 16, 2021, from https://publikasjoner.nve.no/faktaark/2016/faktaark2016_01.pdf

Norges Vassdrag- og Energidirektorat. (2021). *Om snøskredvarslingen.* Retrieved May 27, 2021, from https://www.varsom.no/snoskredvarsling/om-snoskredvarslingen/?ref=mainmenu

Norwegian Meteorological Institute. (n.d.). *WxGen* (Version 0.3.0). Retrieved November 10, 2017, from https://github.com/metno/wxgen/wiki

Pielmeier, C., & Schneebeli, M. (2003). Developments in the stratigraphy of snow. *Surveys in Geophysics*, *24*, 389–416.

Schweizer, J., Bruce Jamieson, J., & Schneebeli, M. (2003). Snow avalanche formation. *Reviews of Geophysics*, *41*(4).

Shi, D., Shi, L., & Chen, T. (2016). *Event-based State Estimation: A Stochastic Perspective* (Vol. 41). Springer International Publishing. https://doi.org/10.1007/978-3-319-26606-0

SINTEF. (n.d.). *Geodrones.* Retrieved May 28, 2021, from https://www.sintef.no/en/projects/2021/geodrones/

Statens Vegvesen. (2014). Veiledning, håndbok v138: Veger og snøskred. Retrieved May 27, 2021, from https://www.vegvesen.no/_attachment/740624/binary/1003961

Viallon-Galinier, L., Hagenmuller, P., Eckert, N., & Reuter, B. (2021). Mechanical stability indicators derived from detailed snow cover simulations. *EGU General Assembly 2021.* https://doi.org/https://doi.org/10.5194/egusphere-egu21-1341

West, M., & Harrison, J. (1997). *Bayesian Forecasting and Dynamic Models.* Springer New York. https://doi.org/10.1007/b98971

WSL Institute for Snow and Avalanche Research SLF. (n.d.-a). *Snow as a material.* Retrieved February 5, 2021, from https://www.slf.ch/en/snow/snow-as-a-material.html

WSL Institute for Snow and Avalanche Research SLF. (n.d.-b). *Snow-cover modelling - snowpack*. Retrieved April 27, 2021, from https://www.slf.ch/en/snow/snowpack/snow-cover-modelling.html

WSL Institute for Snow and Avalanche Research SLF. (n.d.-c). *SNOWPACK* (Version 3.6.0). Retrieved March 14, 2021, from https://models.slf.ch/docserver/snowpack/html/index.html

WSL Institute for Snow and Avalanche Research SLF. (n.d.-d). *Snowpack*. Retrieved February 7, 2021, from https://www.slf.ch/en/snow/snowpack.html

Appendix A

Figures of the weather scenarios.

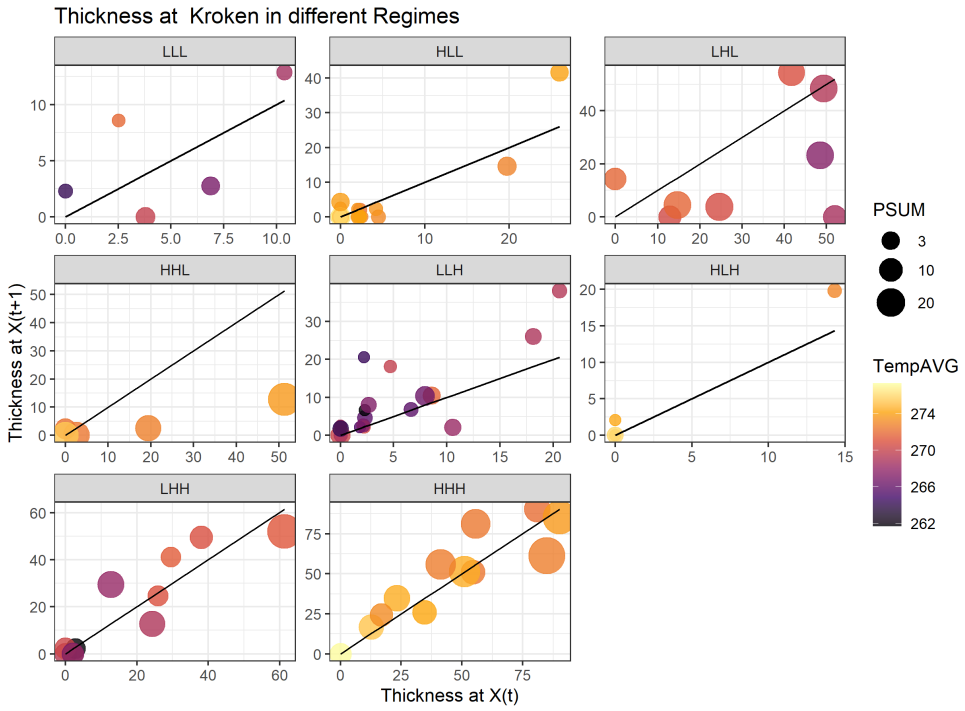

Figure 26: Cross-plot of new snow thickness in different regimes at Kroken.

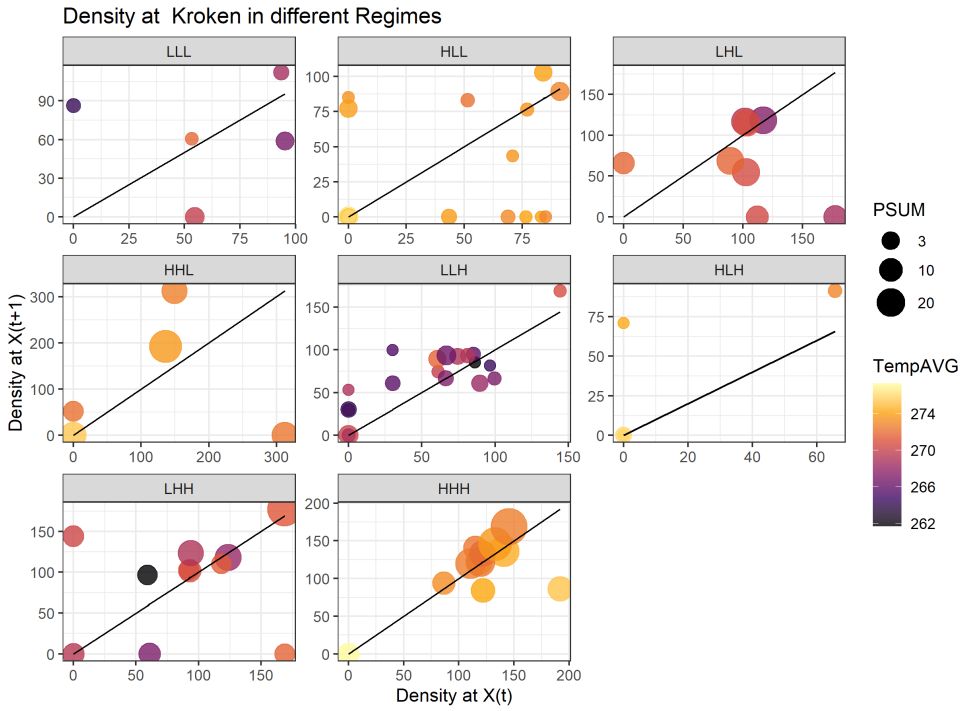

Figure 27: Cross-plot of new snow density in different regimes at Kroken.

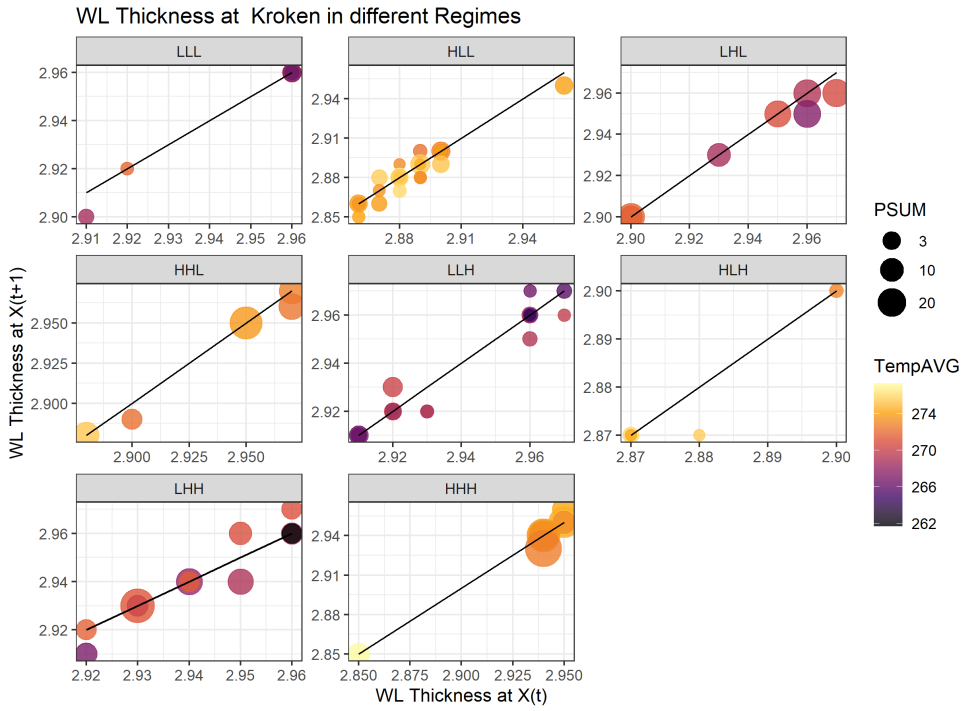

Figure 28: Cross-plot of weak layer thickness in different regimes at Kroken.

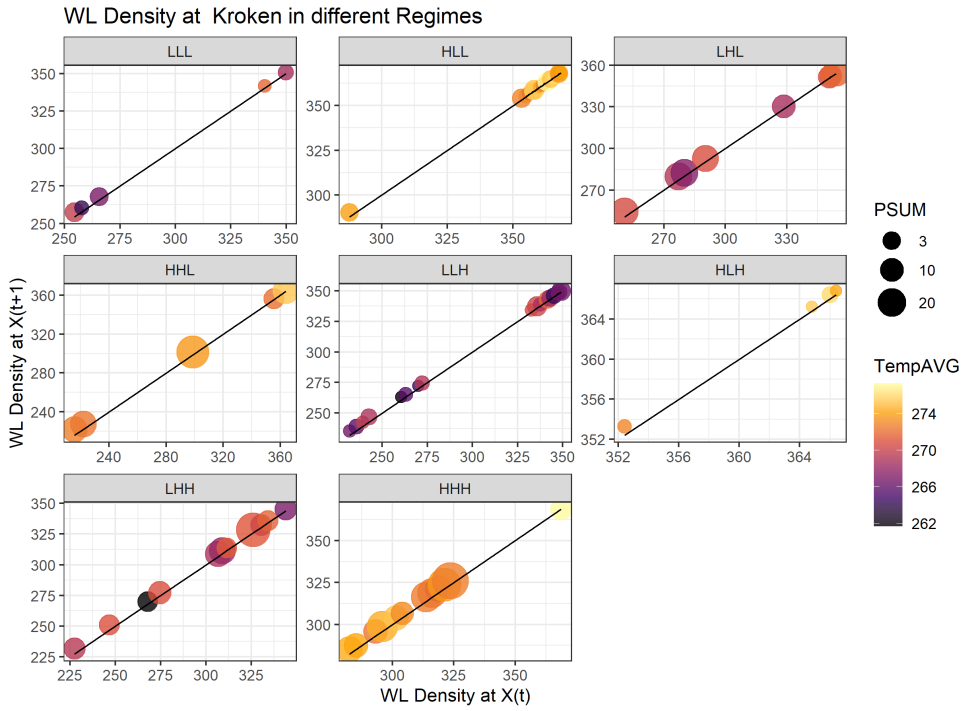

Figure 29: Cross-plot of weak layer density in different regimes at Kroken.

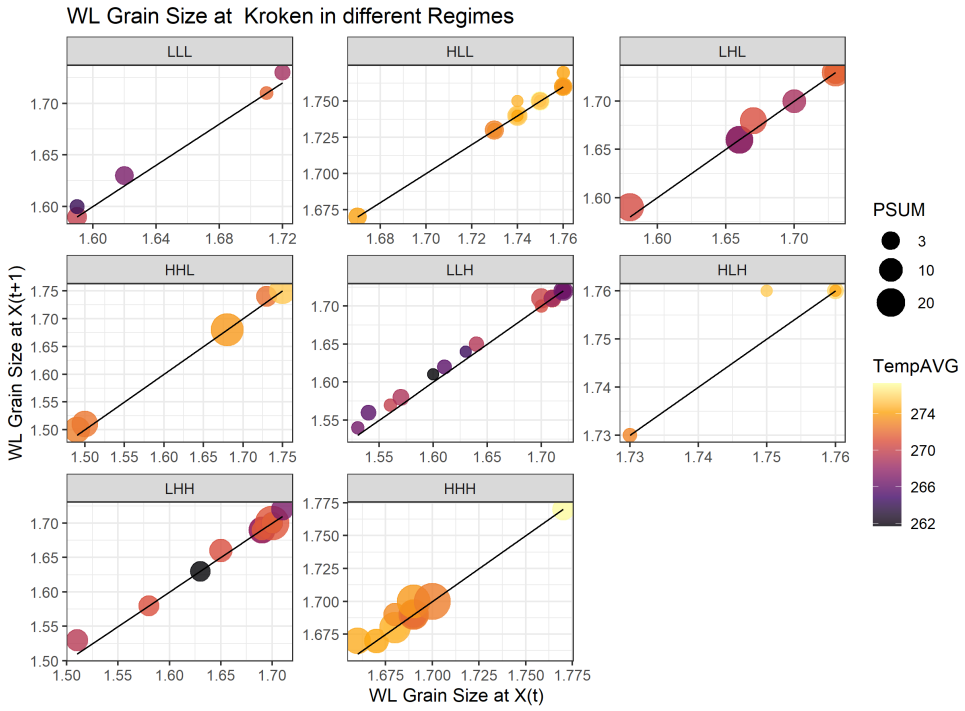

Figure 30: Cross-plot of weak layer grain size in different regimes at Kroken.

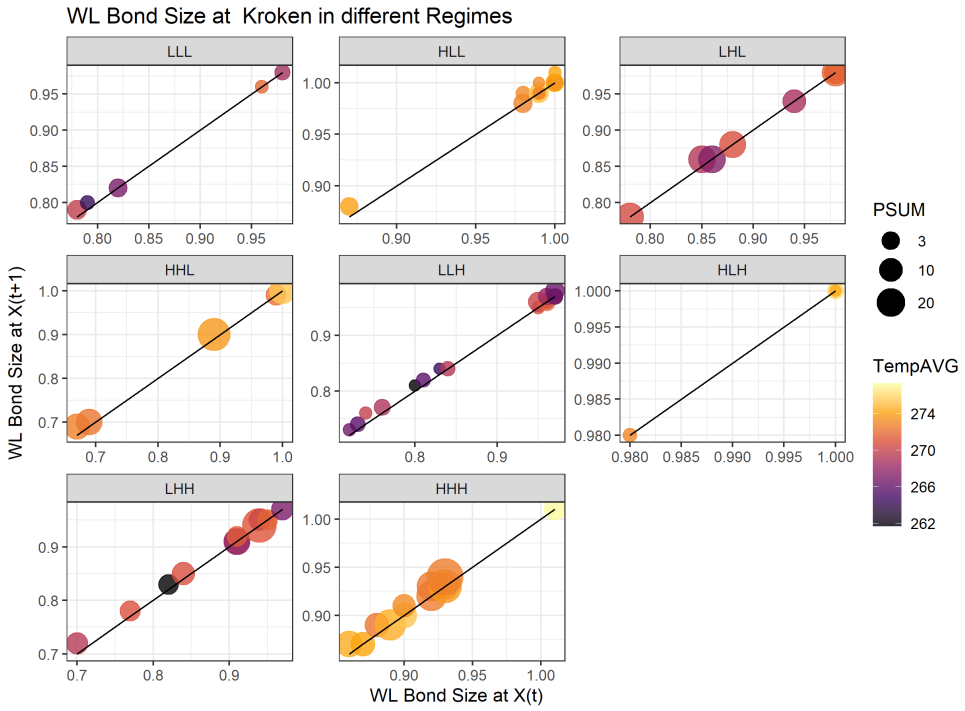

Figure 31: Cross-plot of weak layer bond size in different regimes at Kroken.

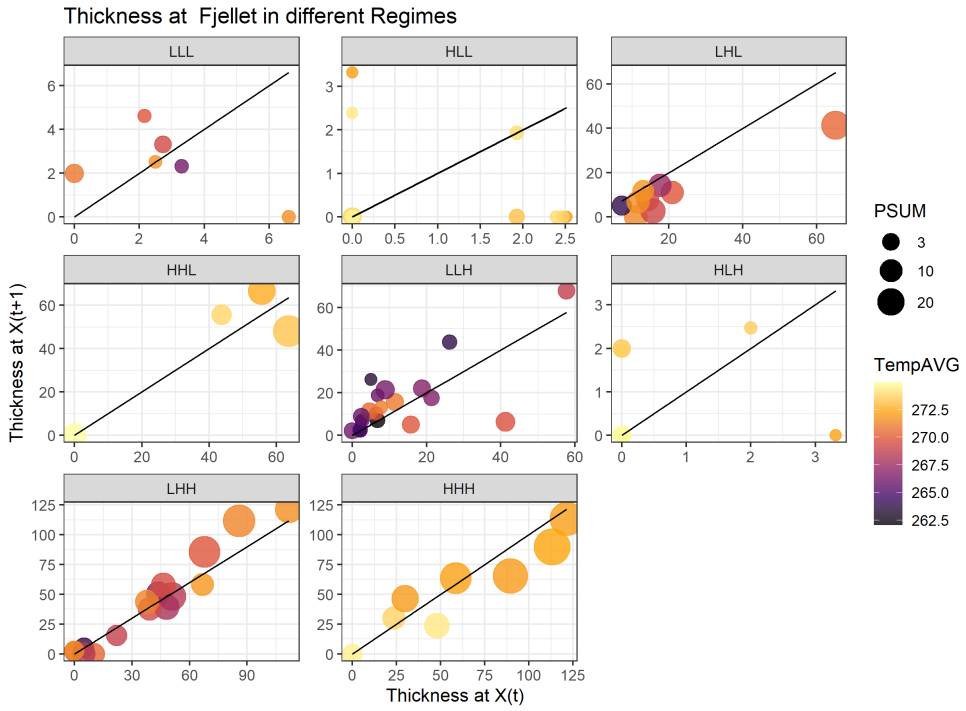

Figure 32: Cross-plot of new snow thickness in different regimes at Fjellet.

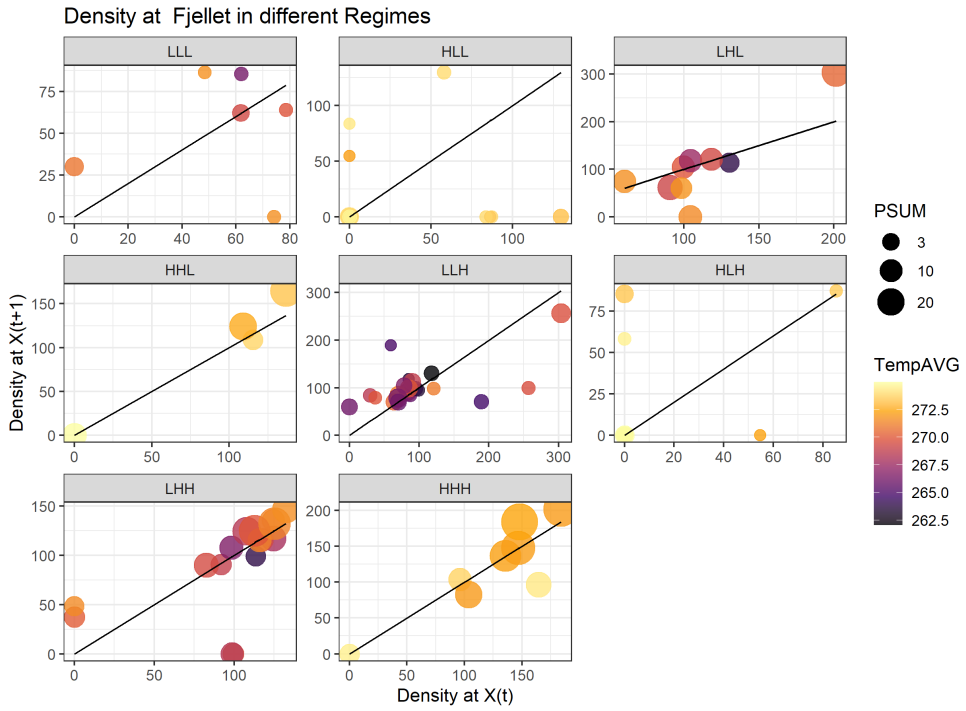

Figure 33: Cross-plot of new snow density in different regimes at Fjellet.

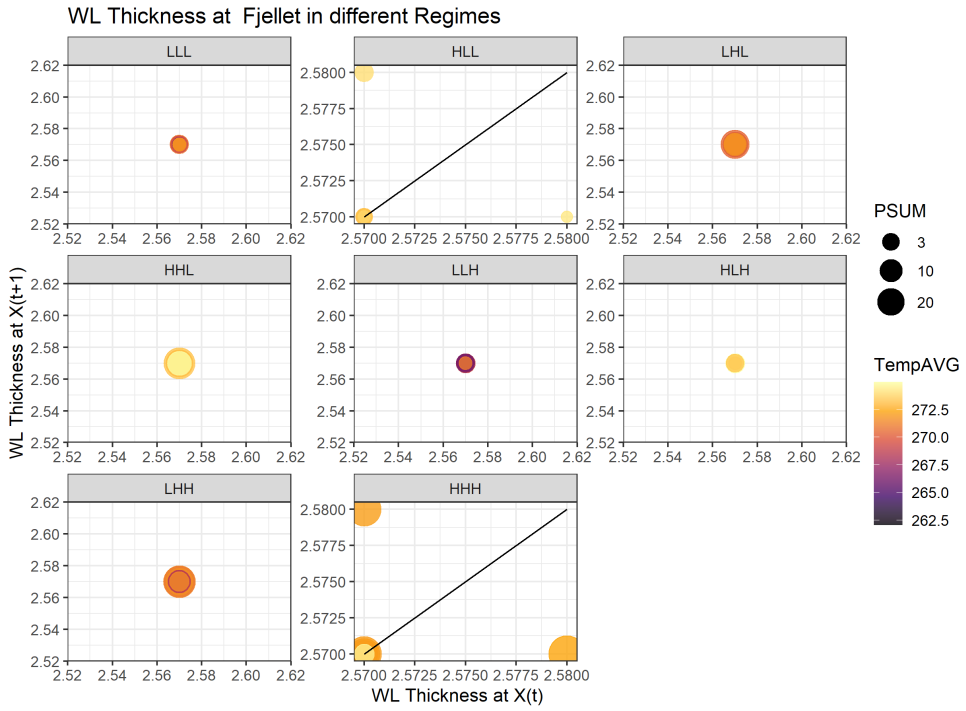

Figure 34: Cross-plot of weak layer thickness in different regimes at Fjellet.

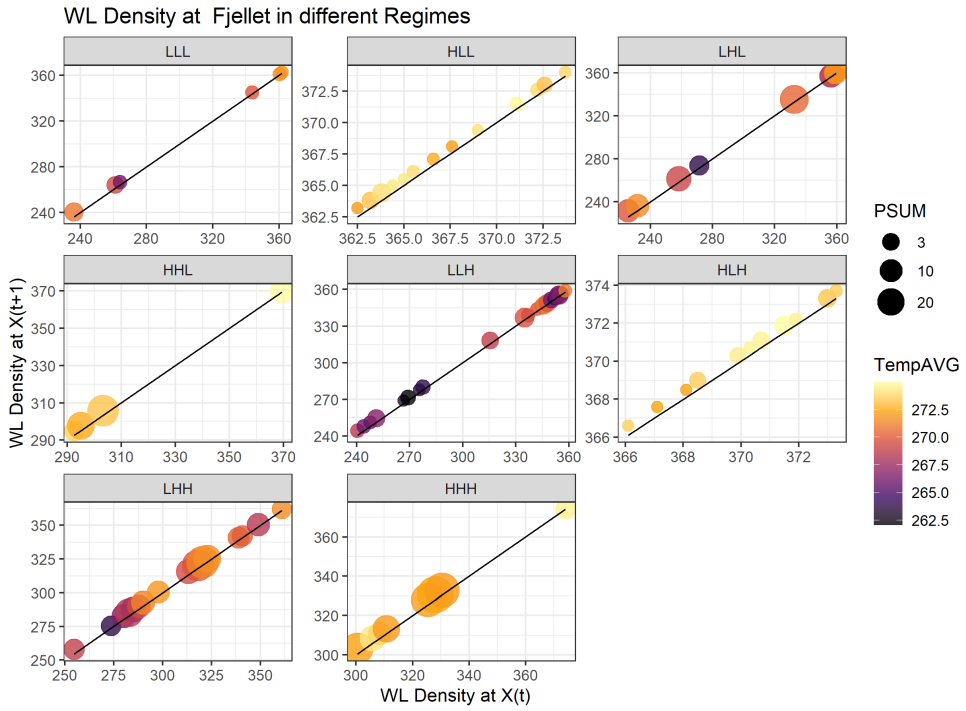

Figure 35: Cross-plot of weak layer density in different regimes at Fjellet.

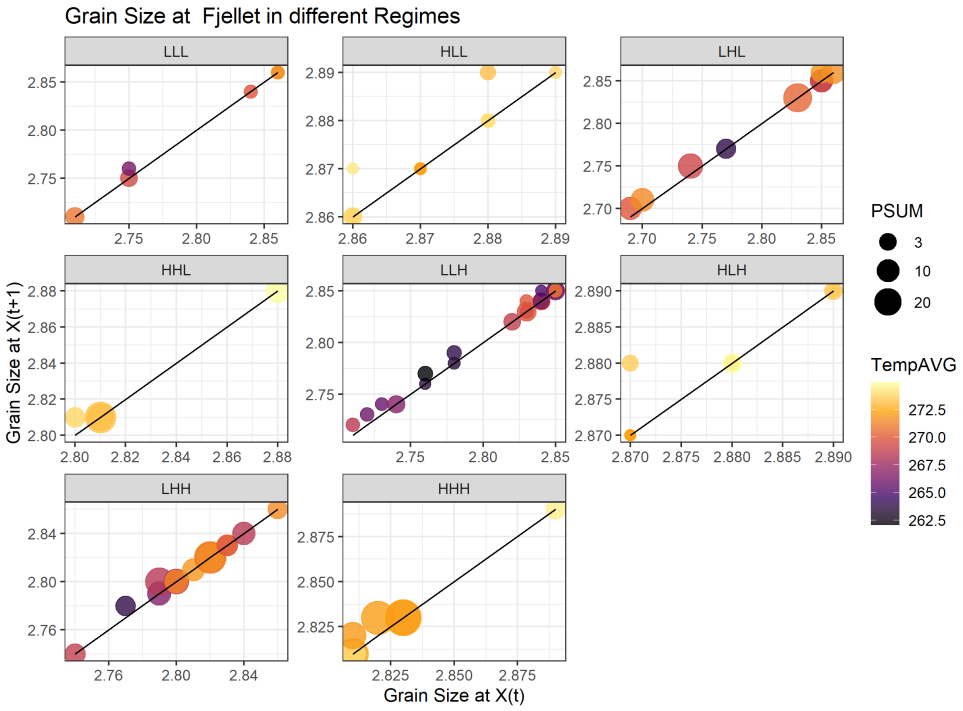

Figure 36: Cross-plot of weak layer grain size in different regimes at Fjellet.

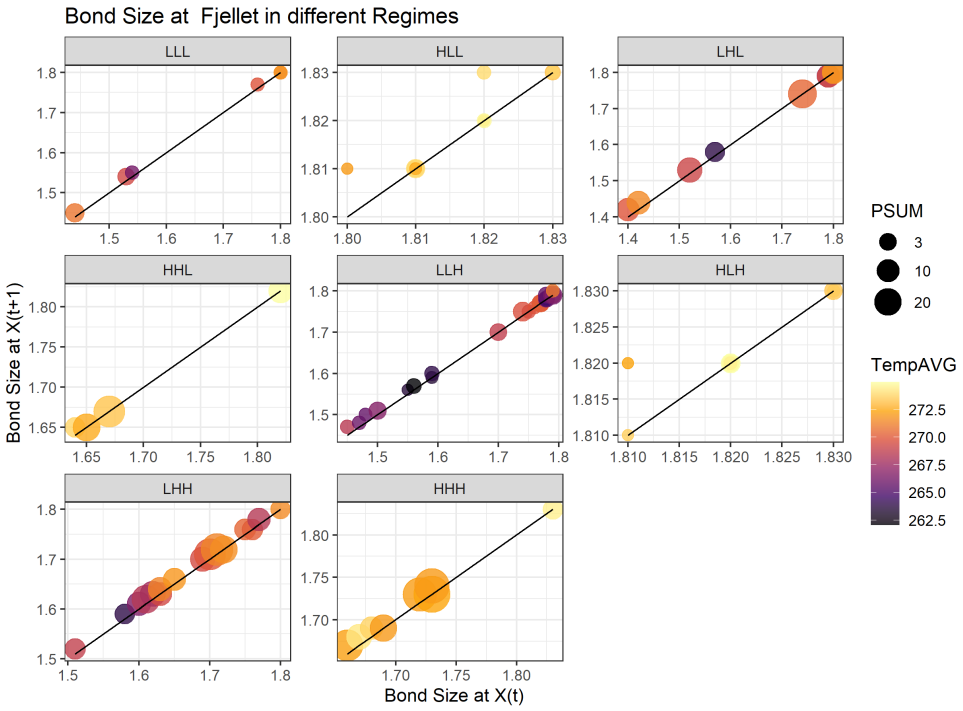

Figure 37: Cross-plot of weak layer bond size in different regimes at Fjellet.

Appendix B

This appendix contains some of the code used to extract and generate the data sets used in the model. This includes the extracting and conversion of data obtained from wxGen, which is used as input for SNOWPACK. It also includes the extraction of data from SNOWPACK, and the grouping of the data into weather regimes.

R-code to extract data from Wxgen (.nc-file):

```
library(ncdf4)
data <- nc_open("name.nc") #.nc file obtained from wxGen.
ts=function(longitude, latitude, data){
  lon <- ncvar_get(data, "longitude")[,1]
  lat <- ncvar_get(data, "latitude")[1,]
  lon.index=which.min(abs(lon-longitude))
  lat.index=which.min(abs(lat-latitude))
  temp = ncvar_get(data, "air_temperature_2m")
  temp_array = array(temp[lon.index, lat.index, ])
  psum = ncvar_get(data, "precipitation_amount") #mm
  psum_array = array(psum[lon.index, lat.index, ])
  xwind = ncvar_get(data, "x_wind_10m") #x-wind
  xwind_array = array(xwind[lon.index, lat.index, ])
  ywind = ncvar_get(data, "y_wind_10m") #y-wind
  ywind_array = array(ywind[lon.index, lat.index, ])
  wind_array = array(dim=length(xwind_array))
  for(i in 1:120){wind_array[i]=sqrt(xwind_array[i]^2+ywind_array[i
     ]^2)}
  isrw = ncvar_get(data, "downwelling_shortwave_flux_in_air") #iswr
  isrw_array = array(isrw[lon.index, lat.index, ])
  df = data.frame(cbind(temp_array, psum_array, wind_array, isrw_
     array))
  return(df)
}
```

R-code to convert from .nc-file to .csv-file format:

```
tocsv=function(lon, lat, data, outputfile){
  df = ts(lon, lat, data)
  csv_path = "" #choose output path of file
  csvname <- outputfile #name of file
  csvfile = paste(csv_path, csvname, sep="")
  write.table(inputdf, csvfile, row.names = FALSE, sep = ",")
}
```

R-code to convert from .xlsx-file to .smet file:

```
my_data = read_excel("filename.xlsx")
dat=data.frame(my_data, row.names = NULL)
write.table(dat, file="sim2loc6376187.smet", row.names=FALSE, col.
    names = FALSE)
```

R-code to extract the snowpack properties of the different layers at Kroken is shown. Similar code was used for Fjellet:

```
library(data.table)
dataKroken=read.csv("SNSTRYN1.csv", sep=",")
#file above is the .pro output from SNOWPACK, converted to .csv-file
#code below extracts specific properties of the different layers in
    the snowpack
densdatakrok= data.frame(setDT(dataKroken, key="X.DATA.")[.(0502)
    ][,-(1:2)]) #density
ssidatakrok= data.frame(setDT(dataKroken, key="X.DATA.")[.(0604)
    ][,-(1:2)]) #ssi
skdatakrok= data.frame(setDT(dataKroken, key="X.DATA.")[.(0533)
    ][,-(1:2)]) #sk38
bondsizekrok=data.frame(setDT(dataKroken, key="X.DATA.")[.(0511)
    ][,-(1:2)]) #bondsize
graindatakrok= data.frame(setDT(dataKroken, key="X.DATA.")[.(0513)
    ][,-(1:2)]) #graintype
heightdatakrok= data.frame(setDT(dataKroken, key="X.DATA.")[.(0501)
    ][,-(1:2)]) #height (for thickness)
grainsizedatakrok= data.frame(setDT(dataKroken, key="X.DATA.")
    [.(0512)][,-(1:2)]) #grainsize
```

R-Code to find the primary grain-type of each layer:

```
for(i in 1:ncol(graindatakrok)){
  for(j in 1:nrow(graindatakrok)){
    graindatakrok[j,i]=substr(graindatakrok[j,i], 0, 1)
}}
```

R-Code to find density of the layers consisting of new snow:

```
denspplayers=matrix(ncol=ncol(densdatakrok), nrow=nrow(densdatakrok)
    )
graindatakrok[graindatakrok==0]=NA
for(j in 1:ncol(densdatakrok)){
  for(i in 1:nrow(densdatakrok)){
    if(graindatakrok[i,j]==1||is.na(graindatakrok[i,j])){
      denspplayers[i,j]=densdatakrok[i,j]
}}}
density=as.matrix(apply(denspplayers, 1, mean, na.rm=TRUE))
density[is.na(density)]=0
density=matrix(density)[-112,] #only include
```

R-Code to find thickness of the layers consisting of new snow:

```
heighpptlayers=matrix(ncol=ncol(densdatakrok), nrow=nrow(
    densdatakrok))
for(j in 1:ncol(heighpptlayers)){
```

```
  for(i in 1:nrow(heighpptlayers)){
    if(graindatakrok[i,j]==1||is.na(graindatakrok[i,j])){
      heighpptlayers[i,j]=heightdatakrok[i,j]
}}}
heightmaxmin=as.matrix(cbind(as.matrix(as.numeric(apply(
   heighpptlayers, 1, hich.min))),as.numeric(apply(heighpptlayers,
   1, which.max))))
thickness = matrix(ncol=1, nrow=111)
thickness[1]=heighpptlayers[1,1]
for(i in 2:nrow(thickness)){
 if(heightmaxmin[i,1]==heightmaxmin[i,2]||is.na(heightmaxmin[i,1])
    ||is.na(heightmaxmin[i,2])){
   tryCatch({
     thickness[i]=heighpptlayers[i,heightmaxmin[i,1]]-(
        heightdatakrok[i, heightmaxmin[i,1]-1])},
            error=function(e){})
 }
 else{thickness[i]=heighpptlayers[i,heightmaxmin[i,2]]-
    heighpptlayers[i,heightmaxmin[i,1]]}
}
thickness[is.na(thickness)]=0
```

Determining the weakest layer of the snowpack (at Kroken) based on the SSI-index, and then extracting properties of the weakest layer:

```
wlkroken= as.matrix(apply(ssidatakrok, 1, which.min))
wlindexkrok=as.numeric(tail(names(sort(table(wlkroken))), 1))
weakestkrok=matrix(0L, nrow = dim(ssidatakrok)[1],ncol=6)
for(i in 1:nrow(weakestkrok)){
  weakestkrok[i,1]=densdatakrok[i, wlindexkrok] #DENSITYWL
  weakestkrok[i,2]=ssidatakrok[i, wlindexkrok] #SSIWL
  weakestkrok[i,3]=abs(heightdatakrok[i, wlindexkrok+1]-
     heightdatakrok[i, wlindexkrok]) #THICKNESSWL
  weakestkrok[i,4]=grainsizedatakrok[i,wlindexkrok] #grainsize
  weakestkrok[i,5]=bondsizekrok[i,wlindexkrok] #bondsize
  weakestkrok[i,6]=skdatakrok[i, wlindexkrok] #SK38
}
```

Extracting weather data (from WxGen) at Kroken:

```
library(readxl)
library(dplyr)
fileinput=read_excel("Krokenweather.xlsx")
#file above is obtained by converting the input to .smet file used
   as input for SNOWPACK into a .xlsx-file
krokenweatherdata = data.frame(fileinput, row.names = NULL)
weatherkroken = matrix(nrow = nrow(krokenweatherdata), ncol= 3)
weatherkroken[1,1]=krokenweatherdata[1,2]
weatherkroken[2,1]=krokenweatherdata[1,2]
weatherkroken[1,2]=0
for(i in 3:nrow(krokenweatherdata)){
  weatherkroken[i,1]=krokenweatherdata[i,2]#temperature
  weatherkroken[i-1,2]=krokenweatherdata[i-2,3] #precipitation
  weatherkroken[i,3]=krokenweatherdata[i,4] #windspeed
```

```
}
```

Function used to regime the data, based on weather, precipitation and wind speed thresholds:

```
#thirdstage is a dataset that contains all the information,
   including weak layer properties, new snow properties and weather
   data for both Kroken and Fjellet.
optim=function(ta, psum, ws){
  for(i in 1:nrow(thirdstage)){
  if(thirdstage[i,8]<=ta & thirdstage[i,9]<=psum & thirdstage[i
     ,10]<=ws){ #LowLowLow
    thirdstage[i,11]=1
  }
  else if(thirdstage[i,8]>ta & thirdstage[i,9]<=psum & thirdstage[i
     ,10]<=ws){ #HighLowLow
    thirdstage[i,11]=2
  }
  else if(thirdstage[i,8]<=ta & thirdstage[i,9]>psum & thirdstage[i
     ,10]<=ws){ #LowHighLow
    thirdstage[i,11]=3
  }
  else if(thirdstage[i,8]>ta & thirdstage[i,9]>psum & thirdstage[i
     ,10]<=ws){ #HighHighLow
    thirdstage[i,11]=4
  }
  else if(thirdstage[i,8]<=ta & thirdstage[i,9]<=psum & thirdstage[i
     ,10]>ws){ #LowLowHigh
    thirdstage[i,11]=5
  }
  else if(thirdstage[i,8]>ta & thirdstage[i,9]<=psum & thirdstage[i
     ,10]>ws){ #HighLowHigh
    thirdstage[i,11]=6
  }
  else if(thirdstage[i,8]<=ta & thirdstage[i,9]>psum & thirdstage[i
     ,10]>ws){ #LowHighHigh
    thirdstage[i,11]=7
  }
  else if(thirdstage[i,8]>ta & thirdstage[i,9]>psum & thirdstage[i
     ,10]>ws){ #HighHighHigh
    thirdstage[i,11]=8
  }}
  return(thirdstage)
}
```

NTNU

Norwegian University of
Science and Technology